

Initial conditions for inflation in an FRW universe

Swagat S. Mishra,^{1,*} Varun Sahni,^{1,†} and Alexey V. Toporensky^{2,3,‡}

¹*Inter-University Centre for Astronomy and Astrophysics, Post Bag 4, Ganeshkhind, Pune 411 007, India*

²*Sternberg Astronomical Institute, Moscow State University,
Universitetsky Prospekt, 13, Moscow 119992, Russia*

³*Kazan Federal University, Kremlevskaya 18, Kazan, 420008, Russia*



(Received 18 April 2018; published 31 October 2018)

We examine the class of initial conditions that give rise to inflation. Our analysis is carried out for several popular models including Higgs inflation, Starobinsky inflation, chaotic inflation, axion-monodromy inflation, and noncanonical inflation. In each case we determine the set of initial conditions that give rise to sufficient inflation, with at least 60 e -foldings. A phase-space analysis is performed for each of these models and the effect of the initial inflationary energy scale on inflation is studied numerically. This paper discusses two scenarios of Higgs inflation: (i) the Higgs is coupled to the scalar curvature, and (ii) the Higgs Lagrangian contains a noncanonical kinetic term. In both cases we find Higgs inflation to be very robust since it can arise for a large class of initial conditions. One of the central results of our analysis is that, for plateau-like potentials associated with the Higgs and Starobinsky models, inflation can be realized even for initial scalar field values that lie close to the *minimum* of the potential. This dispels a misconception related to plateau potentials prevailing in the literature. We also find that inflation in all models is more robust for larger values of the initial energy scale.

DOI: [10.1103/PhysRevD.98.083538](https://doi.org/10.1103/PhysRevD.98.083538)

I. INTRODUCTION

Since its inception in the early 1980s, the inflationary scenario has emerged as a popular paradigm for describing the physics of the very early Universe [1–5]. A major reason for the success of the inflationary scenario is that, in tandem with explaining many observational features of our Universe—including its homogeneity, isotropy, and spatial flatness—it can also account for the existence of galaxies, via the mechanism of tiny initial (quantum) fluctuations which are subsequently amplified through gravitational instability [6–9].

An important issue that needs to be addressed by a successful model of inflation is whether the Universe can inflate starting from a sufficiently large class of initial conditions. This issue was affirmatively answered for chaotic inflation in Refs. [10,11]. Since then, the inventory of inflationary models has rapidly increased. In this paper we attempt to generalize the analysis of Refs. [10,11] to other popular inflationary models, including Higgs inflation, Starobinsky inflation, etc., emphasizing the distinction between power-law potentials and asymptotically flat “plateau-like” potentials. As we will show, our results

for asymptotically flat potentials do not provide support to the “*unlikeliness problem*” raised in Ref. [12].¹

Our paper is organized as follows. We introduce our method of analysis in Sec. II. Section III discusses power-law potentials and includes chaotic inflation and monodromy inflation. Section IV discusses Higgs inflation in the context of both the nonminimal as well as the noncanonical framework.² Section V is devoted to Starobinsky inflation. Our results are presented in Sec. VI.

We work in the units $c, \hbar = 1$ and the reduced Planck mass is assumed to be $m_p = \frac{1}{\sqrt{8\pi G}}$. The metric signature is $(-, +, +, +)$. For simplicity we assume that the preinflationary patch which resulted in inflation was homogeneous, isotropic, and spatially flat. An examination of inflation within a more general cosmological setting can be found in Ref. [15].

II. METHODOLOGY

The action for a scalar field that couples minimally to gravity has the following general form:

$$S[\phi] = \int d^4x \sqrt{-g} \mathcal{L}(F, \phi), \quad (1)$$

¹See Ref. [13] for an analysis of other problems with plateau-like potentials raised in Ref. [12].

²As pointed out in Ref. [14], noncanonical scalars permit the Higgs field to play the role of the inflaton.

*swagat@iucaa.in

†varun@iucaa.in

‡atopor@rambler.ru

where the Lagrangian density $\mathcal{L}(\phi, F)$ is a function of the field ϕ and the kinetic term

$$F = \frac{1}{2} \partial_\mu \phi \partial^\mu \phi. \quad (2)$$

Varying Eq. (1) with respect to ϕ results in the equation of motion

$$\frac{\partial \mathcal{L}}{\partial \phi} - \left(\frac{1}{\sqrt{-g}} \right) \partial_\mu \left(\sqrt{-g} \frac{\partial \mathcal{L}}{\partial (\partial_\mu \phi)} \right) = 0. \quad (3)$$

The energy-momentum tensor associated with the scalar field is

$$T^{\mu\nu} = \left(\frac{\partial \mathcal{L}}{\partial F} \right) (\partial^\mu \phi \partial^\nu \phi) - g^{\mu\nu} \mathcal{L}. \quad (4)$$

Specializing to a spatially flat Friedmann-Robertson-Walker (FRW) universe and a homogeneous scalar field, one gets

$$ds^2 = -dt^2 + a^2(t)[dx^2 + dy^2 + dz^2], \quad (5)$$

$$T^\mu{}_\nu = \text{diag}(-\rho_\phi, p_\phi, p_\phi, p_\phi), \quad (6)$$

where the energy density ρ_ϕ and pressure p_ϕ are given by

$$\rho_\phi = \left(\frac{\partial \mathcal{L}}{\partial F} \right) (2F) - \mathcal{L}, \quad (7)$$

$$p_\phi = \mathcal{L}, \quad (8)$$

and $F = -(\dot{\phi}^2/2)$. The evolution of the scale factor $a(t)$ is governed by the Friedmann equations:

$$\left(\frac{\dot{a}}{a} \right)^2 = \left(\frac{8\pi G}{3} \right) \rho_\phi, \quad (9)$$

$$\frac{\ddot{a}}{a} = - \left(\frac{4\pi G}{3} \right) (\rho_\phi + 3p_\phi), \quad (10)$$

where ρ_ϕ satisfies the conservation equation

$$\dot{\rho}_\phi = -3H(\rho_\phi + p_\phi), \quad H \equiv \frac{\dot{a}}{a}. \quad (11)$$

For a canonical scalar field

$$\mathcal{L}(F, \phi) = -F - V(\phi), \quad (12)$$

Substituting Eq. (12) into Eqs. (7) and (8), we find

$$\rho_\phi = \frac{1}{2} \dot{\phi}^2 + V(\phi), \quad p_\phi = \frac{1}{2} \dot{\phi}^2 - V(\phi). \quad (13)$$

Consequently, the two Friedmann equations (9) and (10) become

$$H^2 = \frac{8\pi G}{3} \left[\frac{1}{2} \dot{\phi}^2 + V(\phi) \right], \quad (14)$$

$$\frac{\ddot{a}}{a} = - \frac{8\pi G}{3} [\dot{\phi}^2 - V(\phi)]. \quad (15)$$

Noting that $\dot{H} + H^2 = \ddot{a}/a$, one finds $\dot{H} = -4\pi G \dot{\phi}^2 < 0$, which informs us that the expansion rate is a monotonically decreasing function of time for canonical scalar fields that couple minimally to gravity. The scalar field equation of motion follows from Eq. (3),

$$\ddot{\phi} + 3H\dot{\phi} + V'(\phi) = 0. \quad (16)$$

Within the context of inflation, a scalar field rolling down its potential is usually associated with the Hubble slow-roll parameters [5]

$$\epsilon_H = 2m_p^2 \left(\frac{H'(\phi)}{H(\phi)} \right)^2, \quad \eta_H = 2m_p^2 \frac{H''(\phi)}{H(\phi)} \quad (17)$$

and the potential slow-roll parameters [5]

$$\epsilon = \frac{m_p^2}{2} \left(\frac{V'}{V} \right)^2, \quad \eta = m_p^2 \frac{V''}{V}. \quad (18)$$

For small values of these parameters $\epsilon_H \ll 1$, $\eta_H \ll 1$, one finds $\epsilon_H \simeq \epsilon$ and $\eta_H \simeq \eta - \epsilon$. The expression for ϵ_H in Eq. (17) can be rewritten as $\epsilon_H = -\frac{\dot{H}}{H^2}$, which implies that the universe accelerates ($\ddot{a} > 0$) when $\epsilon_H < 1$. For the scalar field models discussed in this paper $\dot{H} = -4\pi G \dot{\phi}^2$, so that $\epsilon_H = 4\pi G \dot{\phi}^2 / H^2$, which reduces to $\epsilon_H \simeq \frac{3}{2} \dot{\phi}^2 / V$ when $\dot{\phi}^2 \ll V$.

The slow-roll parameters play an important role in determining the spectral index of scalar perturbations, since³ $n_S - 1 = -6\epsilon + 2\eta$. Observations indicate that $n_S \simeq 0.97$ [16], which suggests that $\epsilon, \eta \ll 1$ on scales associated with the present cosmological horizon. The fact that ϵ, η are required to be rather small might appear to imply that successful inflation can only arise under a very restricted set of initial conditions, namely, those for which $\dot{\phi}^2 / V(\phi) \ll 1$. This need not necessarily be the case. As originally demonstrated in the context of chaotic inflation [10,11], a scalar field rolling down a power-law potential can arrive at the attractor trajectory $\epsilon, \eta \ll 1$ from a very wide range of initial conditions. In this paper we shall apply the methods developed in Refs. [10,11,17] to several inflationary models with power-law and plateau-like

³Here, $n_S - 1 \equiv \frac{d \ln \mathcal{P}_S}{d \ln k}$, where \mathcal{P}_S is the power spectrum of scalar curvature perturbations.

potentials in order to assess the impact of initial conditions on these models.

In addition to the field equations developed earlier, we will find it convenient to work with the parameter

$$N_e = \log \frac{a(t_{\text{end}})}{a(t_{\text{initial}})} = \int_{t_i}^{t_e} H dt \equiv - \int_{\phi_e}^{\phi} \left(\frac{H}{\dot{\phi}} \right) d\phi, \quad (19)$$

which describes the number of inflationary e -foldings since the onset of inflation. For our purpose it will also be instructive to rewrite the Friedman equation (14) as

$$R^2 = X^2 + Y^2, \quad (20)$$

where

$$R = \sqrt{6} \frac{H}{m_p}, \quad X = \hat{\phi} \frac{\sqrt{2V(\phi)}}{m_p^2}, \quad Y = \frac{1}{m_p^2} \frac{d\phi}{dt}, \quad (21)$$

where $\hat{\phi} = \frac{\phi}{|\phi|}$ is the sign of ϕ (this definition ensures that X and ϕ have the same sign). Clearly, by holding R fixed and varying X and Y , one arrives at a set of initial conditions that satisfy the constraint equation (20) defining the boundary of a circle of radius R . Adequate inflation is then qualified by the range of initial values of X and Y for which the universe inflates by at least 60 e -foldings, i.e., $N_e \geq 60$.

We begin our discussion of inflationary models by an analysis of power-law potentials which are usually associated with chaotic inflation [11,18].

III. INFLATION WITH POWER-LAW POTENTIALS

A. Chaotic inflation

We first consider the potential [18]

$$V(\phi) = \frac{1}{2} m^2 \phi^2, \quad (22)$$

where $m \simeq 5.97 \times 10^{-6} m_p$ is assumed, in agreement with observations of the cosmic microwave background (CMB) [16,19] (see Appendix A). The generality of this model is studied by plotting the phase-space diagram (Y vs X) and determining the region of initial conditions which gives rise to $N_e \geq 60$. Equations (15), (16), and (19) have been solved numerically for different initial energy scales H_i . The phase-space diagram corresponding to $H_i = 3 \times 10^{-3} m_p$ is shown in Fig. 1.

To study the effect of different energy scales on inflation, we take different values of R ($\equiv \sqrt{6} H_i / m_p$) and determine the range of initial values of ϕ that lead to adequate inflation with $N_e \geq 60$. [The initial value of $\dot{\phi}$ is conveniently determined from the consistency relation (20).] Our results are summarized in Fig. 3. The solid blue lines correspond to initial values, ϕ_i , which always result in adequate inflation

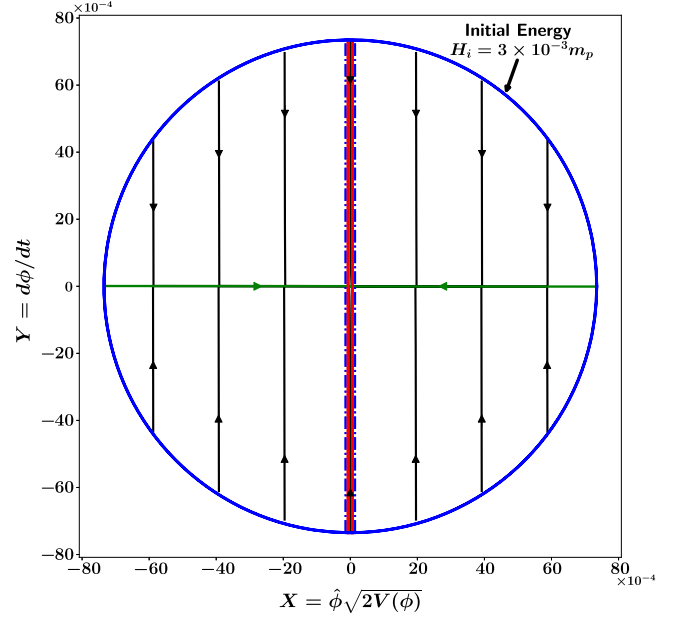


FIG. 1. This figure illustrates the phase-space of chaotic inflation described by the potential (22). Y ($= \dot{\phi}$) is plotted against X ($= \hat{\phi} \sqrt{2V(\phi)}$) for different initial conditions, all of which begin on the circumference of a circle (blue) with radius $R = \sqrt{6} H_i / m_p$ corresponding to the initial energy scale $H_i = 3 \times 10^{-3} m_p$. ($\hat{\phi} = \frac{\phi}{|\phi|}$ is the sign of field ϕ .) One finds that, beginning from the circle, the different inflationary trajectories rapidly converge towards one of the two inflationary separatrices (green horizontal lines). After this, the scalar field moves towards the minimum of the potential $V(\phi)$ at $X = 0$, $Y = 0$. The thin vertical central band (red) corresponds to the region in phase space that *does not* lead to adequate inflation ($N_e < 60$). This central region is shown greatly magnified in Fig. 2.

(irrespective of the sign of $\dot{\phi}_i$). The dashed red lines corresponding to $\phi_i \in [-\phi_B, -\phi_A] \cup [\phi_A, \phi_B]$ result in adequate inflation only when $\dot{\phi}_i$ points in the direction of increasing $V(\phi)$ (represented by blue arrows). Inadequate inflation is associated with the region $\phi_i \in [-\phi_A, \phi_A]$. If the initial scalar field value falls within this region then one does not get adequate inflation *irrespective of the sign* of $\dot{\phi}_i$. This region is shown in Fig. 3 by the solid red line. The dependence of ϕ_A and ϕ_B on the initial energy scale H_i is given in Table I.

To determine the fraction of initial conditions that do not lead to adequate inflation (we call this the “degree of inadequate inflation”), we consider a uniform measure on the distribution of initial conditions for Y_i ($\equiv \dot{\phi}_i$) and X_i ($\equiv \hat{\phi}_i \sqrt{2V(\phi_i)}$). These initial conditions are described by a circle of circumference $l = 2\pi R$ with $R = \sqrt{6} H_i$ (in Planck units), which is illustrated in Fig. 4. The degree of inadequate inflation and marginally adequate inflation (corresponding, respectively, to ϕ_A and ϕ_B in Fig. 3) is $2 \frac{\Delta l_A}{l}$ and $2 \frac{\Delta l_B}{l}$, where Δl_A and Δl_B are illustrated in Fig. 4.

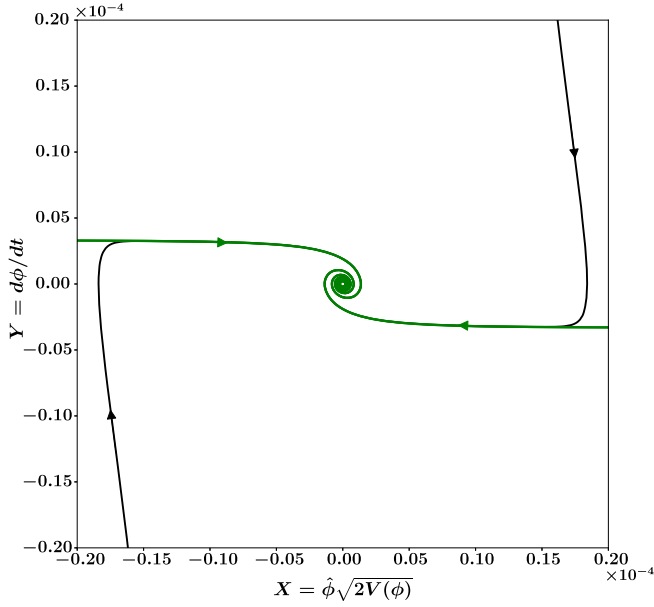


FIG. 2. A zoomed-in view of the central region of Fig. 1. Note that $\hat{\phi} = \frac{\dot{\phi}}{|\dot{\phi}|}$ gives the sign of ϕ . Inflationary trajectories (black) corresponding to different initial values of ϕ and $\dot{\phi}$ first converge onto the slow-roll inflationary separatrices (green horizontal lines) before spiraling towards the center.

The dependence of ϕ_A , ϕ_B and $\frac{\Delta I_A}{I}$, $\frac{\Delta I_B}{I}$ on the beginning scale of inflation is shown in Table I. We see that the fraction of initial conditions that lead to inadequate inflation, $2\frac{\Delta I_A}{I}$, decreases with an increase in the initial energy scale H_i . This result is also illustrated in Figs. 11(a) and 11(b) where we compare chaotic inflation with monodromy inflation.

B. Monodromy inflation

A straightforward extension of chaotic inflation, called axion-monodromy inflation, was discussed in Refs. [20,21] in the context of string theory⁴ and tested against the CMB in Refs. [16,25]. The potential for monodromy inflation, which contains a monomial term along with axionic sinusoidal modulations, is given by

$$V(\phi) = V_0 \left| \frac{\phi}{m_p} \right|^p + \Lambda^4 \left(\cos \frac{\phi}{f} - 1 \right) \quad (23)$$

for $0 < p \leq 1$, where f is the axion decay constant while Λ is the scale corresponding to nonperturbative effects. In this paper our focus will be on two values of p , namely, $p = 1, \frac{2}{3}$. (However, our methods are very general and easily carry over to other values of p .)

Demanding the monotonicity of the potential (23), one gets

⁴See Refs. [22–24] for a field-theory analogue of monodromy inflation.

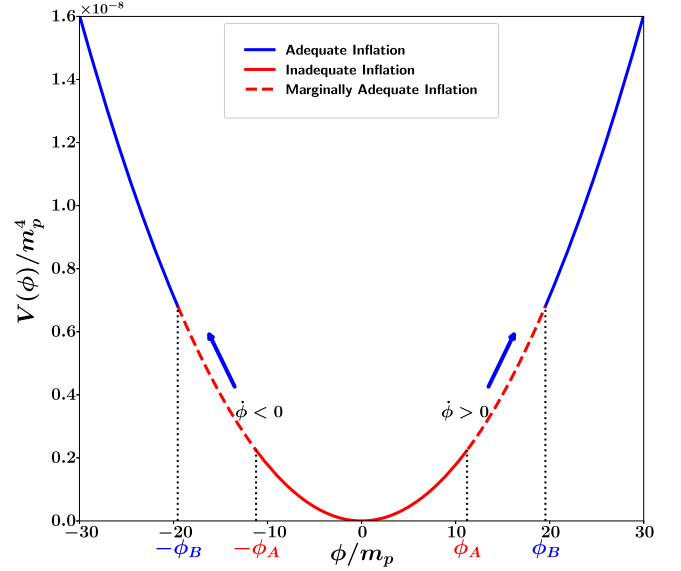


FIG. 3. Initial field values ϕ_i that lead to adequate inflation with $N_e \geq 60$ (blue), marginally adequate inflation (dashed red), and inadequate inflation (red) are schematically shown for chaotic inflation [Eq. (22)]. The blue lines represent regions of adequate inflation. Initial values of ϕ_i lying in the blue region result in adequate inflation *irrespective* of the sign of $\dot{\phi}_i$. The red lines are either dashed or solid and correspond to the following two possibilities. (i) The solid red line represents initial values of ϕ_i for which inflation is never adequate irrespective of the direction of $\dot{\phi}_i$. (ii) In the region shown by the dashed red line one gets adequate inflation only when $\dot{\phi}_i$ is directed towards increasing values of $V(\phi)$ (shown by blue arrows). Note that only a small portion of the full potential is shown in this figure which corresponds to the initial energy scale $H_i = 3 \times 10^{-3} m_p$.

$$b \left| \frac{\phi}{m_p} \right|^{1-p} \sin \frac{\phi}{f} < 1, \quad (24)$$

where $b = \frac{\Lambda^4 m_p}{p V_0 f}$. Since $p \leq 1$ and the observable period of inflation corresponds to $\phi > m_p$, the monotonicity condition (24) implies $b < 1$. Furthermore, for $b < 1$ observational constraints [25] from the CMB (combined with microphysical constraints from string theory) require $b \ll 1$ and $f \ll m_p$. This implies that the amplitude of modulation $\Lambda^4 = V_0 \frac{f}{m_p} b p$ is much smaller than the monomial term, i.e., $\Lambda^4 \ll V_0$. In other words, the sinusoidal axionic term has a negligible effect on the background dynamics so that, in an analysis of inflation, one can safely approximate the potential by its monomial term, namely,⁵

$$V(\phi) = V_0 \left| \frac{\phi}{m_p} \right|^p. \quad (25)$$

⁵Note that for $b \geq 1$, the monodromy potential (23) can have quite complicated but interesting features. However, in this work we shall confine ourselves to the case $b < 1$ as discussed in Refs. [16,25].

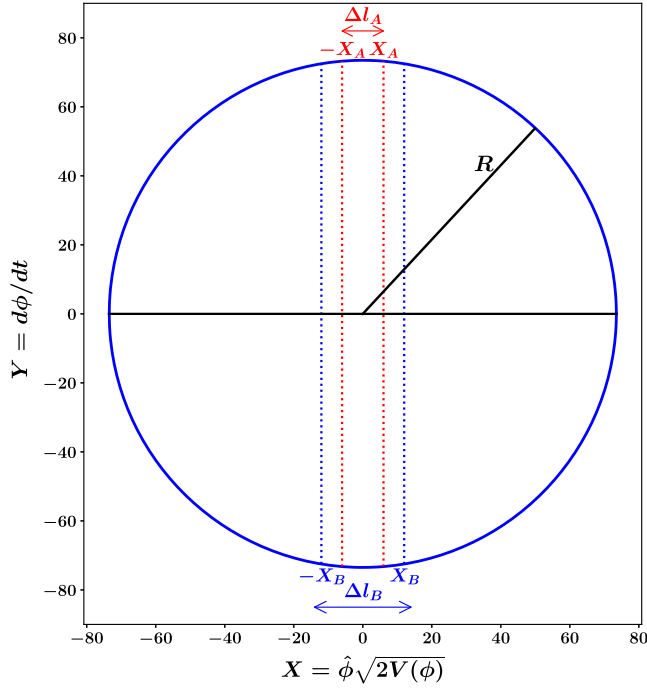


FIG. 4. This figure illustrates how one can determine the degree of adequate/inadequate inflation for power-law potentials characterizing chaotic inflation and monodromy inflation. The fraction of initial conditions (corresponding to ϕ_A and ϕ_B in Fig. 3) that leads either to inadequate inflation or marginally adequate inflation is given by $2 \frac{\Delta l_A}{l}$ and $2 \frac{\Delta l_B}{l}$, respectively, where $l = 2\pi R$. Adequate inflation with $N_e \geq 60$ is described by the fraction $1 - 2 \frac{\Delta l_B}{l}$ ($\hat{\phi} = \frac{\phi}{|\phi|}$ is the sign of field ϕ).

It is important to mention that for $p \leq 1$ the potentials (23) as well as Eq. (25) are not differentiable at the origin. This might lead to problems when ϕ rapidly oscillates around $\phi = 0$ after the end of inflation at $\phi = \phi_{\text{end}}$. We circumvent this problem with the following useful generalization⁶ of Eq. (25):

$$V(\phi) = V_1 \left| \frac{\phi}{\phi_c} \right|^p W(\phi), \quad (26)$$

where $W(\phi) = [1 + (\frac{\phi_c}{\phi})^n]^{\frac{p-2}{n}}$, $V_1 = V_0(\phi_c/m_p)^p$, and $n > 1$ is an integer (we assume $n = 4$ in the ensuing analysis). In this expression the value of ϕ_c is chosen so that $V(\phi) \sim |\phi|^p$ for $|\phi| \gg |\phi_c|$, whereas $V(\phi) \sim \phi^2$ for $|\phi| \ll |\phi_c|$. It is well known that inflation ends when the slow-roll parameter ϵ in Eq. (18) grows to unity. Substituting Eq. (25) into Eq. (18) and setting $\epsilon \simeq 1$, one finds $\phi_{\text{end}} = \frac{p}{\sqrt{2}} m_p$ which can be used as a reference to set a value for ϕ_c , namely, $\phi_c \ll \phi_{\text{end}}$. One should note that the monomial parts of the actual potentials of axion-monodromy inflation for $p = 1, \frac{2}{3}$ do not have cusps at the origin. For example, for

⁶See Ref. [26] for a similar modification of Eq. (25).

TABLE I. Dependence of ϕ_A , ϕ_B , $\frac{\Delta l_A}{l}$, and $\frac{\Delta l_B}{l}$ on the initial energy scale H_i for quadratic chaotic inflation; see Fig. 4. Here $l = 2\pi R \equiv 2\pi\sqrt{6}H_i/m_p$. Note that the fraction of initial conditions that lead to inadequate inflation, $2 \frac{\Delta l_A}{l}$, decreases as H_i is increased. The same is true for the fraction of initial conditions giving rise to marginally adequate inflation, $2 \frac{\Delta l_B}{l}$. The fraction of initial conditions leading to adequate inflation, with $N_e \geq 60$, is given by $1 - 2 \frac{\Delta l_B}{l}$. Thus inflation proves to be more general for larger values of the initial energy scale H_i , since a larger initial region in phase space gives rise to adequate inflation with $N_e \geq 60$.

H_i (in m_p)	ϕ_A (in m_p)	ϕ_B (in m_p)	$2 \frac{\Delta l_A}{l}$	$2 \frac{\Delta l_B}{l}$
3×10^{-3}	11.22	19.55	5.80×10^{-3}	1.01×10^{-2}
3×10^{-2}	9.33	21.38	4.83×10^{-4}	1.11×10^{-3}
3×10^{-1}	7.47	23.27	3.86×10^{-5}	1.20×10^{-4}

$p = 1$ the monomial term has the form [21] $V(\phi) = V_0 \left(\sqrt{(\phi/m_p)^2 + (\phi_c/m_p)^2} - (\phi_c/m_p) \right)$ which displays smooth quadratic behavior near $\phi = 0$. Likewise, for a general value of the monodromy parameter p , it is

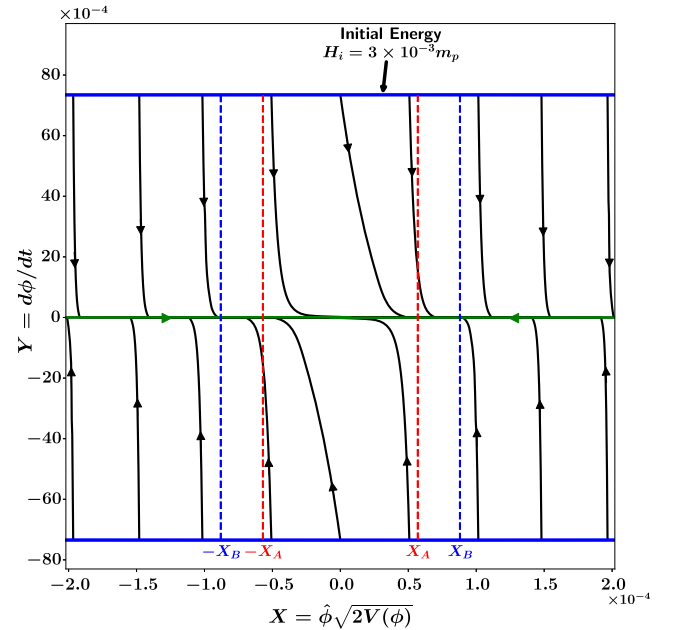


FIG. 5. This figure shows a portion of the phase space of monodromy inflation $V \propto |\phi|$. The variable Y ($= \dot{\phi}$) is plotted against X ($= \hat{\phi} \sqrt{2V(\phi)}$). ($\hat{\phi} = \frac{\phi}{|\phi|}$ is the sign of field ϕ .) The initial conditions are specified on arcs which form the blue colored boundary. Note that these arcs correspond to a *very small portion* of the full “initial conditions” circle R , and therefore appear to be straight lines. In this analysis we assume $R = \sqrt{6}H_i/m_p$, with $H_i = 3 \times 10^{-3} m_p$. We find that, beginning at the boundary, most solutions quickly converge to the two slow-roll inflationary separatrices (green horizontal lines) before traveling to the origin where $\{\phi, \dot{\phi}\} = \{0, 0\}$. A zoomed-in view of the central portion of this figure is shown in Fig. 6.

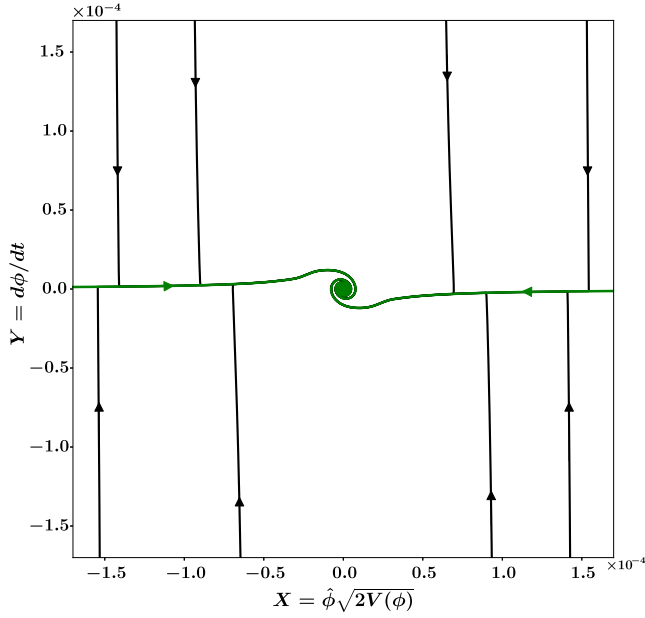


FIG. 6. A zoomed-in view of the phase space of monodromy inflation with $V \propto |\phi|$. Note that scalar field trajectories initially converge towards the slow-roll inflationary separatrices (horizontal green lines), moving from there towards $\phi = 0$, where the field oscillates.

convenient to modify the potential around $\phi = 0$ without changing any of the results for the background dynamics, as done in Ref. [26]. Our introduction of a smoothing kernel W in Eq. (26) follows a similar line of reasoning. It is important to emphasize that our results are quite insensitive to the values of n and ϕ_c in Eq. (26) provided $\phi_c \ll \phi_{\text{end}}$ and $n > 1$.

Next, we proceed with a generality analysis for $p = 1$ which will be followed by a similar analysis for $p = 2/3$.

C. Linear monodromy inflation

Consider first the linear potential

$$V(\phi) = V_0 \left| \frac{\phi}{m_p} \right|, \quad (27)$$

where $V_0 \simeq 1.97 \times 10^{-10} m_p^4$ is in agreement with the CMB [16] (see Appendix A). The phase-space diagram for this potential, shown in Fig. 5, was obtained by solving Eqs. (15), (16), (19), and (27) numerically for the initial energy scale $H_i = 3 \times 10^{-3} m_p$.

Initial values of ϕ that lead to adequate or inadequate inflation are schematically shown in Fig. 7. Inadequate inflation arises when the scalar field originates in the region $\phi_i \in [-\phi_A, \phi_A]$, shown by the solid red line. Blue lines represent initial field values $\phi_i \in (-\phi_m, -\phi_B) \cup (\phi_B, \phi_m)$, which always result in adequate inflation. Note that ϕ_m is the maximum allowed value of ϕ_i for a given initial energy

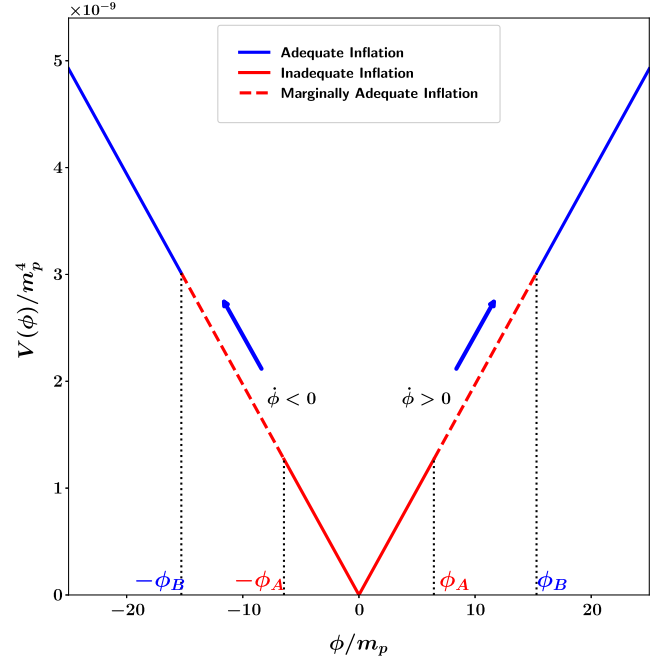


FIG. 7. This figure schematically shows initial field values that result in adequate inflation with $N_e \geq 60$ (blue), marginally adequate inflation (dashed red), and inadequate inflation (red) for the monodromy potential $V \propto |\phi|$. The initial energy scale is $H_i = 3 \times 10^{-3} m_p$. As earlier, blue lines represent regions of adequate inflation. The red lines are either dashed or solid and correspond to the two possible initial directions of $\dot{\phi}$. The solid red line represents initial values of ϕ for which inflation is never adequate irrespective of the direction of $\dot{\phi}_i$. In the region shown by the dashed line one gets adequate inflation only when $\dot{\phi}_i$ points in the direction (shown by blue arrows) of increasing $V(\phi)$. Note that only a small portion of the full potential is shown in this figure.

scale, as determined from the consistency equations (14) and (20). Initial conditions $\phi_i \in [-\phi_B, -\phi_A] \cup [\phi_A, \phi_B]$, shown by dashed red lines, lead to adequate inflation only when $\dot{\phi}_i$ points in the direction (shown by blue arrows) of

TABLE II. Dependence of ϕ_A , ϕ_B , $\frac{\Delta l_A}{l}$, and $\frac{\Delta l_B}{l}$ on the initial energy scale H_i for monodromy inflation $V \propto |\phi|$. Here $l = 2\pi R \equiv 2\pi\sqrt{6}H_i/m_p$ and $\frac{\Delta l_A}{l}$, $\frac{\Delta l_B}{l}$ were defined in Fig. 4. Note that the fraction of initial conditions that lead to inadequate inflation, $2\frac{\Delta l_A}{l}$, decreases as H_i is increased. The same is true for the fraction of initial conditions giving rise to marginally adequate inflation, $2\frac{\Delta l_B}{l}$. The fraction of initial conditions leading to adequate inflation, with $N_e \geq 60$, is given by $1 - 2\frac{\Delta l_B}{l}$. Thus inflation proves to be more general for larger values of the initial energy scale H_i , since a larger initial region in phase space gives rise to adequate inflation with $N_e \geq 60$.

H_i (in m_p)	ϕ_A (in m_p)	ϕ_B (in m_p)	$2\frac{\Delta l_A}{l}$	$2\frac{\Delta l_B}{l}$
3×10^{-3}	6.45	15.29	4.37×10^{-3}	6.73×10^{-3}
3×10^{-2}	4.58	17.18	3.68×10^{-4}	7.13×10^{-4}
3×10^{-1}	2.69	19.06	2.84×10^{-5}	7.51×10^{-5}

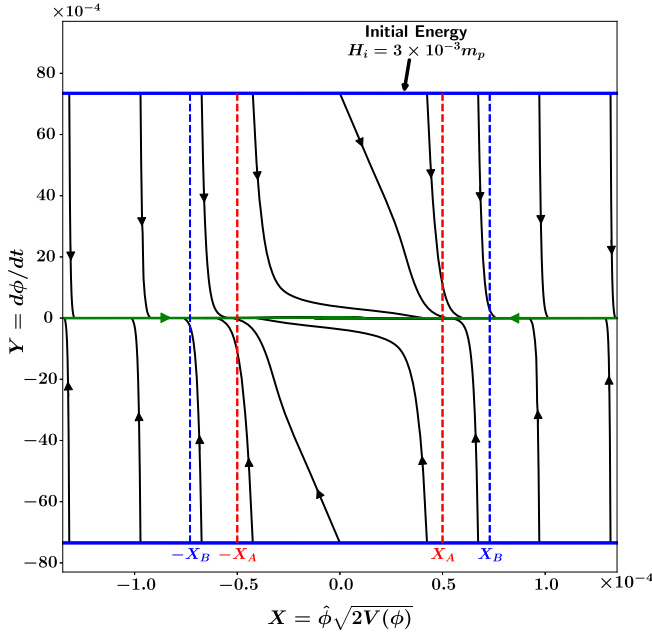


FIG. 8. This figure shows a portion of the phase space of monodromy inflation with $V \propto |\phi|^{2/3}$. The variable Y ($= \dot{\phi}$) is plotted against X ($= \hat{\phi} \sqrt{2V(\phi)}$). ($\hat{\phi} = \frac{\phi}{|\phi|}$ is the sign of field ϕ .) Initial conditions are specified on arcs which form the blue colored boundary. Note that since these arcs correspond to a *very small portion* of the full “initial conditions” circle R , they appear to be straight lines. As in the previous analysis for chaotic inflation we again assume $R = \sqrt{6}H_i/m_p$, with $H_i = 3 \times 10^{-3}m_p$. One finds that, beginning at the boundary, most solutions quickly converge to the two slow-roll inflationary separatrices (green horizontal lines) before traveling to the origin where $\{\phi, \dot{\phi}\} = \{0, 0\}$. A zoomed-in view of the central portion of this figure is shown in Fig. 9.

increasing $V(\phi)$. The dependence of ϕ_A and ϕ_B on the initial energy scale H_i is shown in Table II.

The values of $2\frac{\Delta l_A}{l}$ and $2\frac{\Delta l_B}{l}$ in Table II have been determined by assuming a uniform distribution of initial values of $Y = \dot{\phi}$ and $X = \hat{\phi} \sqrt{2V(\phi)}$ on the circular boundary (20). We find that $2\frac{\Delta l_A}{l}$ and $2\frac{\Delta l_B}{l}$ decrease with an increase in H_i , as expected.

D. Fractional monodromy inflation

Next we consider

$$V(\phi) = V_0 \left| \frac{\phi}{m_p} \right|^{2/3}, \quad (28)$$

where CMB constraints imply $V_0 = 3.34 \times 10^{-10} m_p^4$ [16] (see Appendix A). The phase-space diagram for this potential, shown in Fig. 8, was obtained by solving Eqs. (15), (16), and (19) numerically for the initial energy scale $H_i = 3 \times 10^{-3}m_p$.

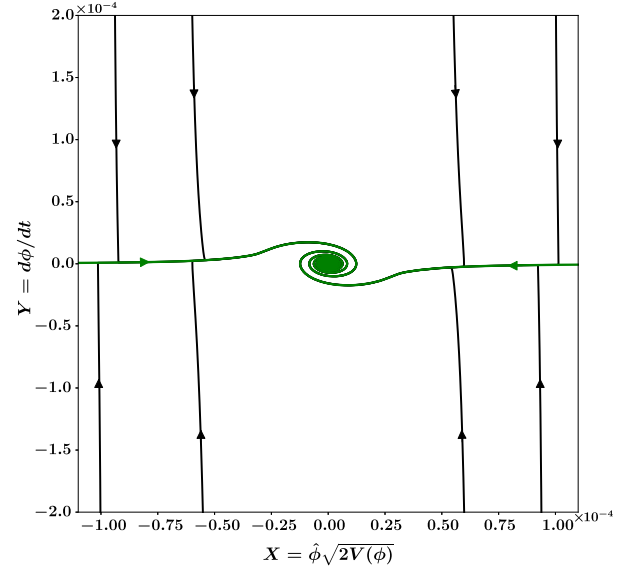


FIG. 9. A zoomed-in view of the phase space of monodromy inflation with $V \propto |\phi|^{2/3}$. One notes that the motion of the scalar field is initially towards the slow-roll inflationary separatrices (horizontal green lines) and from there towards $\phi = 0$, where the field oscillates.

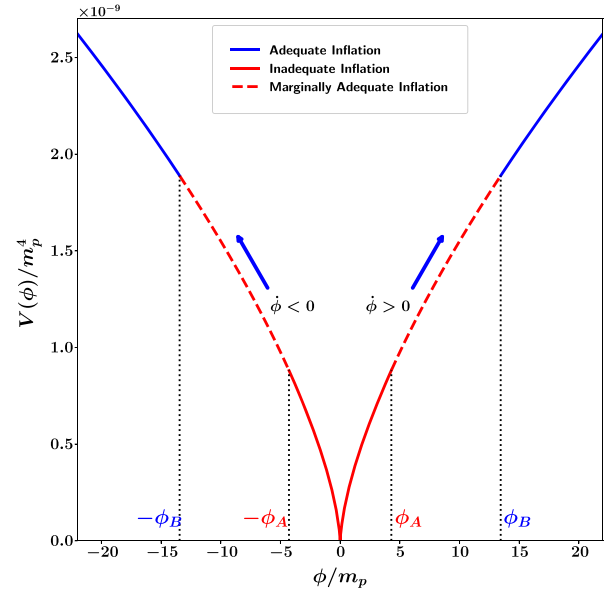


FIG. 10. This figure schematically shows initial field values which result in adequate inflation with $N_e \geq 60$ (blue), marginally adequate inflation (dashed red), and inadequate inflation (red) for the monodromy potential (28). The initial energy scale is $H_i = 3 \times 10^{-3}m_p$. As earlier, blue lines represent regions of adequate inflation. The red lines are either dashed or solid and correspond to the two possible initial directions of $\dot{\phi}$. The solid red line represents initial values of ϕ for which inflation is never adequate irrespective of the direction of $\dot{\phi}_i$. In the region shown by the dashed red line one gets adequate inflation only when $\dot{\phi}_i$ points in the direction (shown by blue arrows) of increasing $V(\phi)$. Note that only a small portion of the full potential is shown in this figure.

TABLE III. Dependence of ϕ_A , ϕ_B , $\frac{\Delta l_A}{l}$, and $\frac{\Delta l_B}{l}$ on the initial energy scale H_i for monodromy inflation with $p = \frac{2}{3}$. Here $l = 2\pi R \equiv 2\pi\sqrt{6}H_i/m_p$ and $\frac{\Delta l_A}{l}$, $\frac{\Delta l_B}{l}$ were defined in Fig. 4. Note that the fraction of initial conditions that lead to inadequate inflation, $2\frac{\Delta l_A}{l}$, decreases as H_i is increased. The same is true for the fraction of initial conditions giving rise to marginally adequate inflation, $2\frac{\Delta l_B}{l}$. The fraction of initial conditions leading to adequate inflation, with $N_e \geq 60$, is given by $1 - 2\frac{\Delta l_B}{l}$. Thus inflation proves to be more general for larger values of the initial energy scale H_i , since a larger initial region in phase space gives rise to adequate inflation with $N_e \geq 60$.

H_i (in m_p)	ϕ_A (in m_p)	ϕ_B (in m_p)	$2\frac{\Delta l_A}{l}$	$2\frac{\Delta l_B}{l}$
3×10^{-3}	4.29	13.45	3.64×10^{-3}	5.33×10^{-3}
3×10^{-2}	2.41	15.33	3.0×10^{-4}	5.56×10^{-4}
3×10^{-1}	0.61	17.22	2.08×10^{-5}	5.78×10^{-5}

Initial values of ϕ that lead to adequate or inadequate inflation are schematically shown in Fig. 10. Inadequate inflation arises when the scalar field originates in the region $\phi_i \in [-\phi_A, \phi_A]$, shown by solid red lines. Blue lines represent initial field values $\phi_i \in (-\phi_m, -\phi_B) \cup (\phi_B, \phi_m)$, which always result in adequate inflation. Note that ϕ_m is the maximum allowed value of ϕ for a given initial energy scale, as determined from the consistency equations (14) and (20). The initial conditions $\phi_i \in [-\phi_B, -\phi_A] \cup [\phi_A, \phi_B]$, shown by dashed red lines, lead to adequate inflation only when $\dot{\phi}_i$ points in the direction (shown by blue arrows) of increasing $V(\phi)$. We refer to this as marginally adequate

inflation. The dependence of ϕ_A and ϕ_B on the initial energy scale H_i is shown in Table III.

As in the case of chaotic inflation, we determine the fraction of initial conditions that do not lead to adequate inflation (the degree of inadequate inflation) by assuming a uniform distribution of initial values of $Y = \dot{\phi}$ and $X = \hat{\phi} \sqrt{2V(\phi)}$ on the circular boundary (14) and (20) with $V(\phi)$ given by Eq. (28). Our results are given in Table III. As was the case for quadratic chaotic inflation, we once more find that $\frac{\Delta l_A}{l}$ and $\frac{\Delta l_B}{l}$ decrease with an increase in H_i ; see Table III, and Figs. 11(a) and 11(b).

E. Comparison of power-law potentials

In this subsection we compare the generality of inflation for the power-law family of potentials, $V \propto |\phi|^p$, by plotting the fraction of initial conditions that *do not lead to adequate inflation* ($2\frac{\Delta l_A}{l}$ and $2\frac{\Delta l_B}{l}$) in Figs. 11(a) and 11(b); also see Tables I–III. These figures demonstrate that the set of initial conditions that give rise to adequate inflation (with $N_e \geq 60$) increases with the energy scale of inflation, H_i . We also find that inflation is sourced by a larger set of initial conditions for the monodromy potential $V \propto |\phi|^{\frac{5}{3}}$, which is followed by $V \propto |\phi|$ and $V \propto \phi^2$, respectively. Finally, we draw attention to the fact that our conclusions remain unchanged if we determine the degree of inflation by a different measure such as $\frac{\Delta \phi_A}{\phi_{\max}}$ and $\frac{\Delta \phi_B}{\phi_{\max}}$, where ϕ_{\max} is the maximum allowed value of ϕ for a given inflationary energy scale.

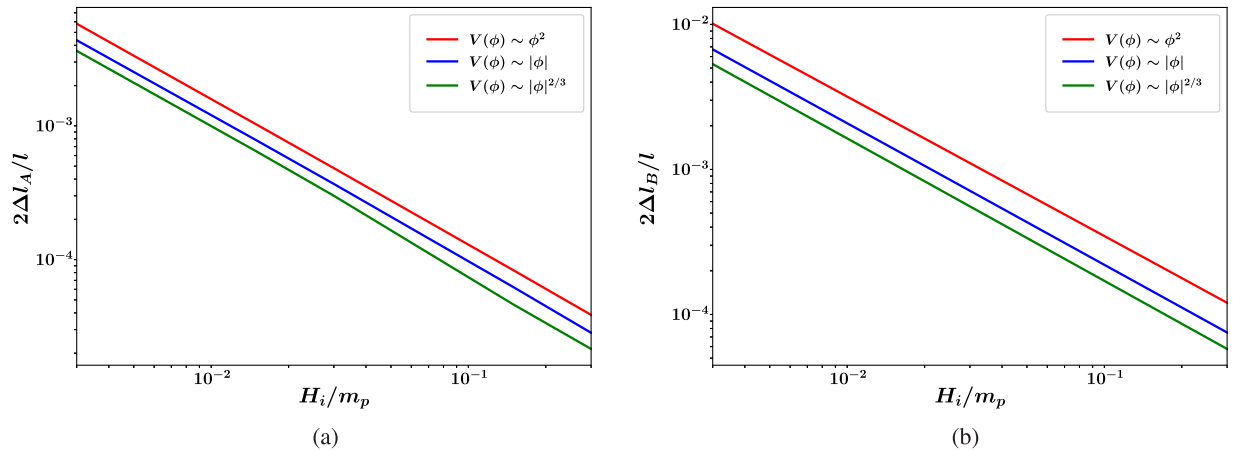


FIG. 11. This figure shows the fraction of initial conditions that lead to (a) inadequate inflation ($2\frac{\Delta l_A}{l}$) and (b) marginally adequate inflation ($2\frac{\Delta l_B}{l}$) plotted against the initial energy scale of inflation H_i . For the definition of $\frac{\Delta l_A}{l}$ and $\frac{\Delta l_B}{l}$, see Fig. 4. The red curve shows results for $V \propto \phi^2$ while the blue and green curves represent monodromy potentials with $V \propto |\phi|$, $|\phi|^{2/3}$, respectively. The decrease in $2\frac{\Delta l_A}{l}$ and $2\frac{\Delta l_B}{l}$, which accompanies an increase in H_i , is indicative of the fact that the set of initial conditions that give rise to adequate inflation (with $N_e \geq 60$) increases with the energy scale of inflation, H_i . This figure also demonstrates that inflation is sourced by a larger set of initial conditions for the monodromy potential $V \propto |\phi|^{\frac{5}{3}}$, which is followed by $V \propto |\phi|$ and finally $V \propto \phi^2$.

IV. HIGGS INFLATION

It would undoubtedly be interesting if inflation could be realized within the context of the Standard Model (SM) of particle physics. Since the SM has only a single scalar degree of freedom, namely, the Higgs field, one can ask whether the Higgs field (30) can source inflation. Unfortunately, the self-interaction coupling of the Higgs field [λ in Eq. (30)] is far too large to be consistent with the small amplitude of scalar fluctuations observed in the cosmic microwave background [16].

This situation can however be remedied if either of the following possibilities is realized: (i) the Higgs couples nonminimally to gravity, or (ii) the Higgs field is described by a noncanonical Lagrangian.⁷

Indeed, as first demonstrated in Ref. [28], inflation can be sourced by the SM Higgs potential if the Higgs field is assumed to couple nonminimally to the Ricci scalar. The resultant inflationary model provides a good fit to observations and has been extensively developed and examined in Refs. [28–32]. A different means of sourcing inflation through the Higgs field was discussed in Ref. [14] where it was shown that the SM Higgs potential with a noncanonical kinetic term fits the CMB data very well by accounting for the currently observed values of the scalar spectral index n_s and the tensor-to-scalar ratio r . We shall proceed to study Higgs inflation first in the nonminimal framework in Sec. IV A, followed by the same in the noncanonical framework in Sec. IV E.

A. Initial conditions for Higgs inflation in the nonminimal framework

Inflation sourced by the SM Higgs boson was first discussed in Ref. [28]. In this model the Higgs nonminimally couples to gravity with a moderate value of the nonminimal coupling⁸ [29,30]. The model does not require an additional degree of freedom beyond the SM and fits the observational data quite well [16]. Reheating after inflation in this model has been studied in detail [30,31,33] and quantum corrections to the potential at very high energies have been shown to be small [32]. In this section we assess the generality of Higgs inflation (in the Einstein frame) and determine the range of initial conditions that give rise to adequate inflation (with $N_e \geq 60$) for a given value of the initial energy scale.

B. Action for Higgs inflation

The action for a scalar field ϕ that couples nonminimally to gravity (i.e., in the Jordan frame) is given by [28,29,34]

$$S_J = \int d^4x \sqrt{-g} \left[f(\phi)R - \frac{1}{2}g^{\mu\nu}\partial_\mu\phi\partial_\nu\phi - U(\phi) \right], \quad (29)$$

where R is the Ricci scalar and $g_{\mu\nu}$ is the metric in the Jordan frame. The potential for the SM Higgs field is given by

$$U(\phi) = \frac{\lambda}{4}(\phi^2 - \sigma^2)^2, \quad (30)$$

where σ is the vacuum expectation value of the Higgs field,

$$\sigma = 246 \text{ GeV} = 1.1 \times 10^{-16} m_p, \quad (31)$$

and the Higgs coupling constant has the value $\lambda = 0.1$. Furthermore,

$$f(\phi) = \frac{1}{2}(m^2 + \xi\phi^2), \quad (32)$$

where m is a mass parameter given by [34]

$$m^2 = m_p^2 - \xi\sigma^2.$$

ξ is the nonminimal coupling constant whose value

$$\xi = 1.62 \times 10^4 \quad (33)$$

agrees with observations [16] (see Appendix A). For the above values⁹ of σ and ξ , one finds $m \simeq m_p$, so that

$$f(\phi) \simeq \frac{1}{2}(m_p^2 + \xi\phi^2) = \frac{m_p^2}{2} \left(1 + \frac{\xi\phi^2}{m_p^2} \right). \quad (34)$$

We now transfer to the Einstein frame by means of the following conformal transformation of the metric [34]:

$$g_{\mu\nu} \rightarrow \hat{g}_{\mu\nu} = \Omega^2 g_{\mu\nu}, \quad (35)$$

where the conformal factor is given by

$$\Omega^2 = \frac{2}{m_p^2} f(\phi) = 1 + \frac{\xi\phi^2}{m_p^2}. \quad (36)$$

After the field redefinition $\phi \rightarrow \chi$ the action in the *Einstein frame* is given by [34]

$$S_E = \int d^4x \sqrt{-\hat{g}} \left[\frac{m_p^2}{2} \hat{R} - \frac{1}{2} \hat{g}^{\mu\nu} \partial_\mu \chi \partial_\nu \chi - V(\chi) \right], \quad (37)$$

where

⁷Another means of reconciling the $\frac{1}{4}\lambda\phi^4$ ($\lambda \sim 0.1$) potential with observations is through a field derivative coupling with the Einstein tensor of the form $G^{\mu\nu}\partial_\mu\partial_\nu\phi/M^2$. This approach has been discussed in Ref. [27].

⁸The value of the dimensionless nonminimal coupling $\xi \sim 10^4$, though quite large, is much smaller than the ratio $(\frac{m_p}{M_W})^2 \simeq 10^{34}$, where $M_W \sim 100$ GeV is the electroweak scale.

⁹Note that the observed vacuum expectation value of the Higgs field $\sigma = 1.1 \times 10^{-16} m_p$ is much smaller than the energy scale of inflation and hence we neglect it in our subsequent calculations.

$$V(\chi) = \frac{U[\phi(\chi)]}{\Omega^4} \quad (38)$$

and

$$\frac{\partial \chi}{\partial \phi} = \pm \frac{1}{\Omega^2} \sqrt{\Omega^2 + \frac{6\xi^2 \phi^2}{m_p^2}}. \quad (39)$$

Equation (37) describes general relativity in the presence of a minimally coupled scalar field χ with the potential $V(\chi)$. (The full derivation of the action in the Einstein frame is given in Appendix B.)

C. Limiting cases of the potential in the Einstein frame

From Eqs. (36) and (39) one finds the following asymptotic forms for the potential (38) (for details see Appendix C and Refs. [28,30]):

(1) For $\phi \ll \sqrt{\frac{2}{3}} \frac{m_p}{\xi}$, one finds

$$\chi = \pm \phi, \quad V(\chi) \simeq \frac{\lambda}{4} \chi^4, \quad |\chi| \ll \sqrt{\frac{2}{3}} \frac{m_p}{\xi}. \quad (40)$$

(2) For $\sqrt{\frac{2}{3}} \frac{m_p}{\xi} \ll \phi \ll \frac{m_p}{\sqrt{\xi}}$

$$\chi = \pm \sqrt{\frac{3}{2}} \frac{\xi \phi^2}{m_p}, \quad V(\chi) \simeq \left(\frac{\lambda m_p^2}{6\xi^2} \right) \chi^2,$$

$$\sqrt{\frac{2}{3}} \frac{m_p}{\xi} \ll |\chi| \ll \sqrt{\frac{3}{2}} m_p. \quad (41)$$

(3) For $\phi \gg \frac{m_p}{\sqrt{\xi}}$

$$\chi = \pm \sqrt{6} m_p \log \left(\frac{\sqrt{\xi} \phi}{m_p} \right),$$

$$V(\chi) \simeq \frac{\frac{\lambda m_p^4}{4\xi^2}}{\left(1 + \exp \left[-\sqrt{\frac{2}{3}} \frac{|\chi|}{m_p} \right] \right)^2},$$

$$|\chi| \gg \sqrt{\frac{3}{2}} m_p. \quad (42)$$

A good analytical approximation to the potential which can accommodate both Eqs. (41) and (42) is

$$V(\chi) \simeq V_0 \left(1 - \exp \left[-\sqrt{\frac{2}{3}} \frac{|\chi|}{m_p} \right] \right)^2, \quad |\chi| \gg \sqrt{\frac{2}{3}} \frac{m_p}{\xi}, \quad (43)$$

where V_0 is given by (Appendix A)

$$V_0 = \frac{\lambda m_p^4}{4\xi^2} = 9.6 \times 10^{-11} m_p^4. \quad (44)$$

D. Generality analysis of Higgs inflation in the Einstein frame

As we have seen, Higgs inflation in the Einstein frame can be described by a minimally coupled canonical scalar field χ with a suitable potential $V(\chi)$. We have analyzed two different limits of the potential $V(\chi)$ which is asymptotically flat and has plateau-like arms for $|\chi| \gg 1$. One notes that when $|\chi| \rightarrow 0$, $V(\chi)$ has a tiny kink with amplitude $\frac{\lambda}{4} \sigma^4 \sim 10^{-66} m_p^4$. This kink is much smaller than the maximum height of the potential and can be neglected for all practical purposes. (This is simply a reflection of the fact that the inflation energy scale is much larger than the electroweak scale.) We have numerically evaluated the potential defined in Eqs. (38) and (39) and compared it with the approximate form given in Eq. (43); see Fig. 12. The difference between the two potentials is shown in Fig. 13. One finds that the maximum fractional difference between the two potentials is only 0.16% which justifies the use of Eq. (43) for further analysis.

During Higgs inflation, the slow-roll parameter is given by

$$\epsilon = \frac{m_p^2}{2} \left(\frac{1}{V} \frac{dV}{d\chi} \right)^2 = \frac{4}{3} \frac{1}{\left(\exp \left(\sqrt{\frac{2}{3}} \frac{|\chi|}{m_p} \right) - 1 \right)^2}, \quad (45)$$

and since slow roll ends when $\epsilon \simeq 1$, one finds

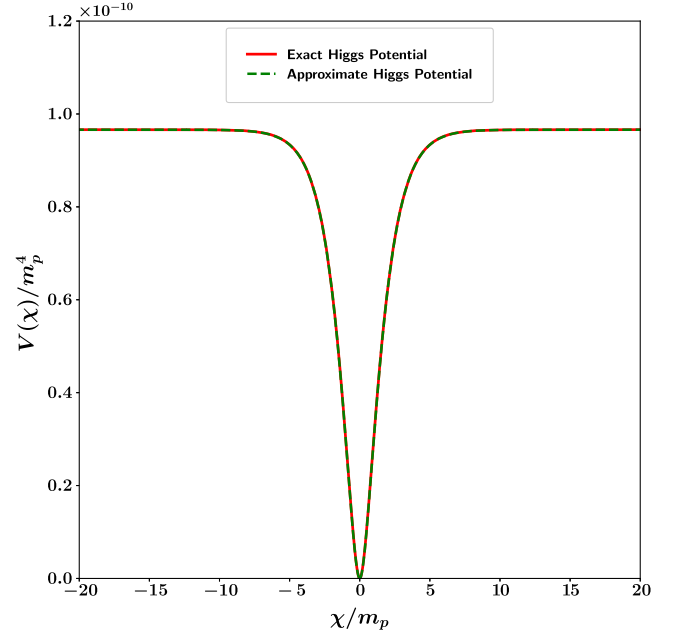


FIG. 12. This figure shows the potential for Higgs inflation (in the Einstein frame) in units of m_p^4 . The (solid) red curve shows the numerically determined value of the potential from Eqs. (38) and (39), while the (dashed) green curve shows the approximate potential $V(\chi) = V_0 \left(1 - \exp \left[-\sqrt{\frac{2}{3}} \frac{|\chi|}{m_p} \right] \right)^2$. Clearly the approximate form matches the exact one very well.

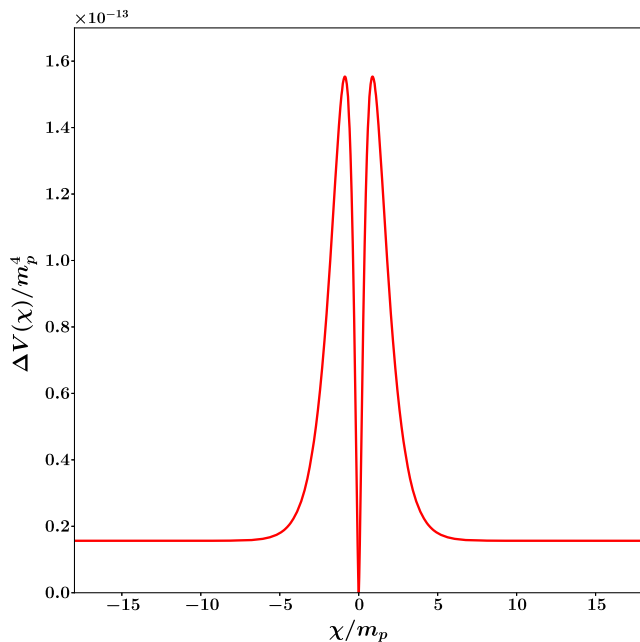


FIG. 13. This figure shows the absolute value of the difference between the numerically determined Higgs potential (38)–(39) and the approximate form (43). We see that the maximum difference is near $\chi \sim m_p$ and its fractional value is only 0.16%.

$$|\chi| \simeq 0.94m_p \sim m_p.$$

We study the generality of Higgs inflation in the Einstein frame by plotting the phase-space diagram for the potential (43) and determining the region of initial conditions that lead to adequate inflation (i.e., $N_e \geq 60$). Our results are shown in Fig. 14 and a zoomed-in view is presented in Fig. 15.

We see that the phase-space diagram for Higgs inflation has very interesting properties. The asymptotically flat arms result in robust inflation, as expected. However, it is also possible to obtain adequate inflation if the inflaton begins from $\chi \simeq 0$. This is because the scalar field is able to climb up the flat wings of $V(\chi)$. This property is illustrated in Fig. 14 by lines originating in the central region, which are slanted and hence can converge to the slow-roll inflationary separatrices resulting in adequate inflation. This feature is not shared by chaotic inflation where one cannot obtain adequate inflation by starting from the origin (provided the initial energy scale is not too large, i.e., $H_i < m_p$.)

However, this does not imply that all possible initial conditions lead to adequate inflation in the Higgs scenario. As shown in Fig. 16, there is a small region of initial field values denoted by $|\chi_A| < |\chi_i| < |\chi_B|$ that does not lead to adequate inflation if χ_i and $\dot{\chi}_i$ have opposite signs (dashed red lines). By contrast, the solid blue lines in the same figure show the region of χ_i that results in adequate inflation *independently of the direction* of the initial velocity $\dot{\chi}_i$. The dependence of χ_A and χ_B on the initial

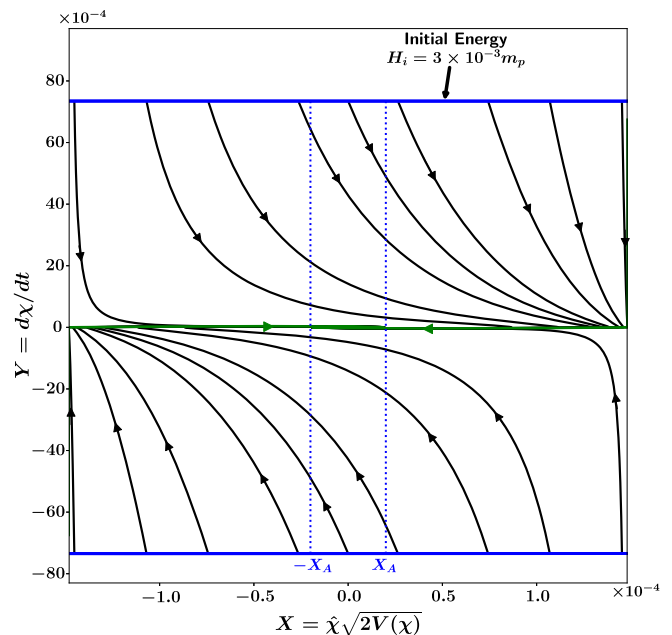


FIG. 14. This figure shows the phase space of Higgs inflation in the Einstein frame. $Y = d\chi/dt$ is plotted against $X = \hat{\chi} \sqrt{2V(\chi)}$ for the initial energy scale $H_i = 3 \times 10^{-3} m_p$. ($\hat{\chi} = \frac{\chi}{m_p}$ is the sign of field χ .) We see that, beginning from a fixed initial energy (shown by the blue boundary lines), most solutions rapidly converge towards the two inflationary separatrices (horizontal green lines) corresponding to slow-roll inflation. We therefore find that inflation for the Higgs potential is remarkably general and can begin from a very wide class of initial conditions. Note that trajectories lying close to the origin, i.e., within the vertical band marked by $(-X_A, X_A)$, are *strongly curved*. This property allows them to converge to the inflationary separatrices giving rise to adequate inflation with $N_e \geq 60$. It is interesting to contrast this behavior with that of chaotic inflation, shown in Fig. 1, for which there is a small region with inadequate inflation near the center. Because of this property, the Higgs scenario displays adequate inflation over a slightly larger range of initial conditions when compared with chaotic inflation.

energy scale is shown in Table IV (also see Fig. 16). Note the surprising fact that the value of $\chi_B - \chi_A$ remains *virtually unchanged* as H_i increases.

The results of Figs. 14, 15, and 16 lead us to conclude that there is a region lying close to the origin of $V(\chi)$, namely, $\chi_i \in (-\chi_A, \chi_A)$, where one gets adequate inflation regardless of the direction of $\dot{\chi}_i$. One might note that this feature is absent in the power-law family of potentials described in the previous section (compare Fig. 16 with Figs. 3, 7, and 10). We therefore conclude that a wide range of initial conditions can generate adequate inflation in the Higgs case,¹⁰ which does not support some of the conclusions drawn in Ref. [12].

¹⁰See Refs. [35,36] for an analysis of classical and quantum initial conditions for Higgs inflation.

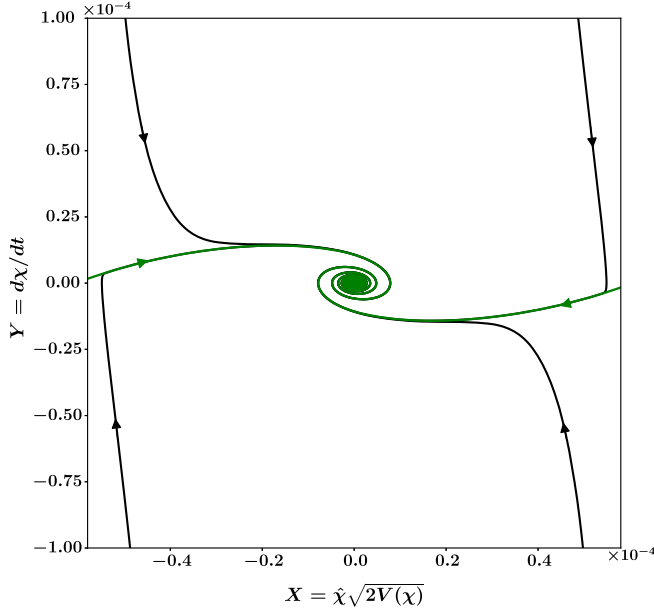


FIG. 15. A zoomed-in view of the central region in Fig. 14. We see that most trajectories (associated with different initial conditions) initially converge towards the horizontal slow-roll inflationary separatrix (green lines) before spiraling in towards the center. (The spiral reflects oscillations of the inflaton about the minimum of its potential.)

Finally, we would like to draw attention to the fact that the phase-space analysis performed here for Higgs inflation is likely to carry over to the T-model α -attractor potential [37], since the two potentials are qualitatively very similar.

E. Initial conditions for Higgs inflation in the noncanonical framework

The class of initial conditions leading to sufficient inflation widens considerably if we choose to work with scalar fields possessing a noncanonical kinetic term.

The Lagrangian for this class of models is [38]

$$\mathcal{L}(\phi, F) = -F \left(\frac{F}{M^4} \right)^{\alpha-1} - V(\phi), \quad (46)$$

where $F = \frac{1}{2} \partial_\mu \phi \partial^\mu \phi$, M has the dimensions of mass, and α is a dimensionless parameter. The associated energy density and pressure in a FRW universe are given by [14,38]

$$\rho_\phi = -(2\alpha - 1)F \left(\frac{F}{M^4} \right)^{\alpha-1} + V(\phi), \quad (47)$$

$$p_\phi = -F \left(\frac{F}{M^4} \right)^{\alpha-1} - V(\phi), \quad F = -\frac{1}{2} \dot{\phi}^2, \quad (48)$$

which reduce to the canonical forms $\rho_\phi = -F + V$, $p_\phi = -F - V$ when $\alpha = 1$. The two Friedmann equations now acquire the forms

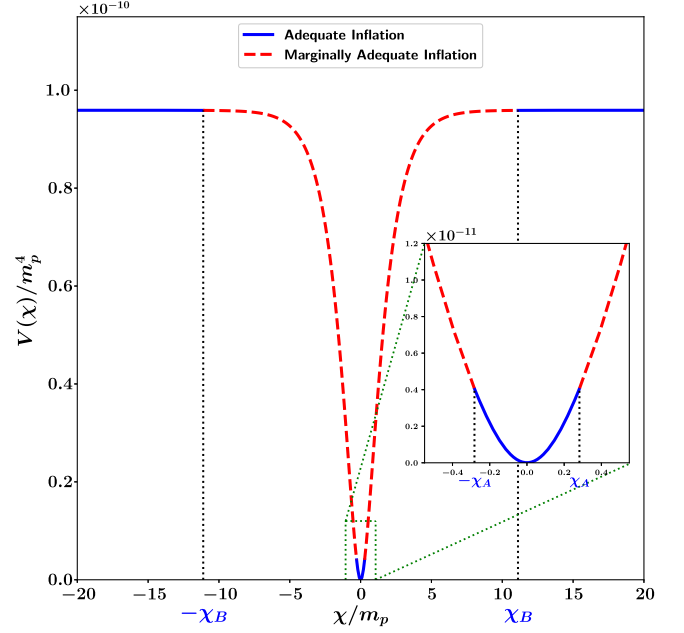


FIG. 16. This figure shows initial field values χ_i that either lead to adequate inflation (solid blue lines) or partially adequate inflation (dashed red lines). The region corresponding to $\chi_i \in [-\chi_B, -\chi_A] \cup [\chi_A, \chi_B]$ (dashed red lines) leads to partially adequate inflation. Initial field values originating in this region result in inadequate inflation only when χ_i is directed towards decreasing values of $V(\chi)$. The alternative case, with χ_i directed towards increasing $V(\chi)$, leads to adequate inflation for the same subset $\chi_i \in [-\chi_B, -\chi_A] \cup [\chi_A, \chi_B]$. This figure is shown for an initial energy scale $H_i = 3 \times 10^{-3} m_p$. The precise values of χ_A and χ_B depend on the initial energy scale H_i , as shown in Table IV. Note that only a small portion of the full potential is shown in this figure.

$$H^2 = \frac{8\pi G}{3} \left[-(2\alpha - 1)F \left(\frac{F}{M^4} \right)^{\alpha-1} + V(\phi) \right], \quad (49)$$

$$\frac{\ddot{a}}{a} = -\frac{8\pi G}{3} \left[-(\alpha + 1)F \left(\frac{F}{M^4} \right)^{\alpha-1} - V(\phi) \right], \quad (50)$$

and the equation of motion of the scalar field becomes

$$\ddot{\phi} + \frac{3}{2\alpha - 1} H \dot{\phi} + \left(\frac{V'(\phi)}{\alpha(2\alpha - 1)} \right) \left(\frac{2M^4}{\dot{\phi}^2} \right)^{\alpha-1} = 0, \quad (51)$$

which reduces to Eq. (16) when $\alpha = 1$.

TABLE IV. Dependence of χ_A and χ_B on the initial energy scale H_i for Higgs inflation (also see Fig. 16).

H_i (in m_p)	χ_A (in m_p)	χ_B (in m_p)	$\chi_B - \chi_A$ (in m_p)
3×10^{-3}	0.28	11.11	10.83
3×10^{-2}	2.16	12.99	10.83
3×10^{-1}	4.04	14.87	10.83

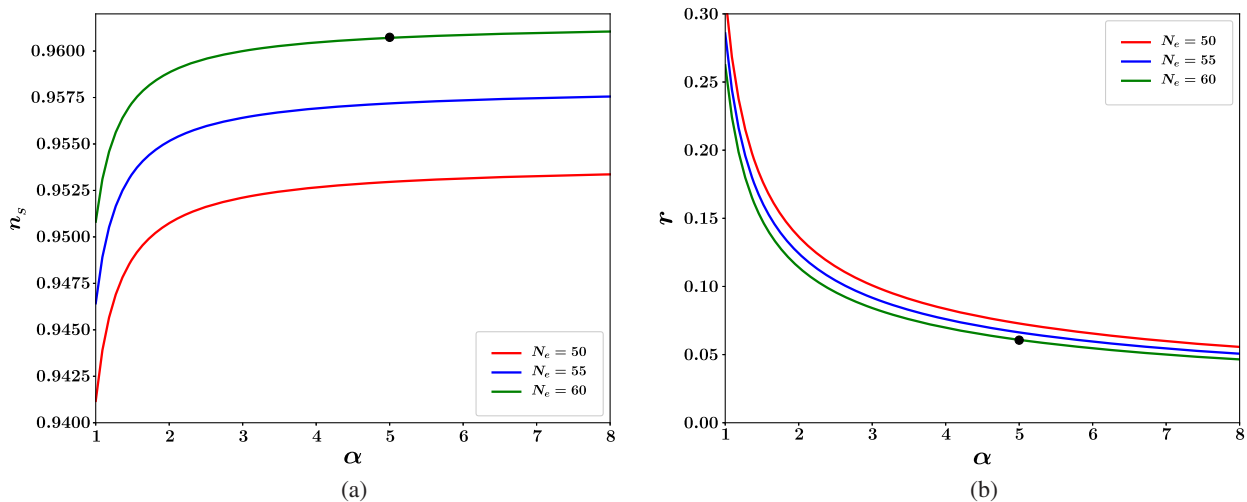


FIG. 17. This figure shows (a) the scalar spectral index n_s and (b) the tensor-to-scalar ratio r as functions of the noncanonical parameter α and described, respectively, by Eqs. (54) and (56). Three values of the number of e -foldings, $N_e = 50, 55,$ and 60 , are chosen. One finds that larger values of α result in higher values of n_s and lower values of r . The black dot in both figures indicates the value of α , and the corresponding values of n_s and r , used in our subsequent analysis.

Before discussing Higgs inflation in the noncanonical framework, we first examine the inflationary slow-roll parameter ϵ_{nc} which, for noncanonical inflation, is given by [14]

$$\epsilon_{nc} = \left(\frac{1}{\alpha}\right)^{\frac{1}{2\alpha-1}} \left(\frac{3M^4}{V}\right)^{\frac{\alpha-1}{2\alpha-1}} (\epsilon_c)^{\frac{\alpha}{2\alpha-1}}, \quad (52)$$

where ϵ_c is the canonical slow-roll parameter (18). Note that $\epsilon_{nc} < \epsilon_c$ for $3M^4 \ll V$. This suggests that for a fixed

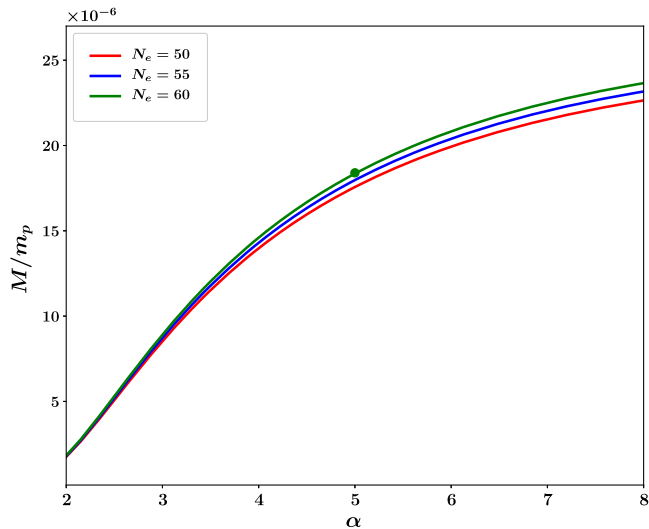


FIG. 18. This figure illustrates the relation between the noncanonical parameters M and α , given by Eq. (57), which results in the self-coupling value $\lambda = 0.1$ in Eq. (53). Results for three different e -folding values $N_e = 50, 55, 60$ are shown. The green dot indicates the values of M and α that are used in our subsequent analysis.

potential V , the duration of inflation can be enhanced relative to the canonical case ($\alpha = 1$) by a suitable choice of M .

1. The higgs potential

It is well known that the standard model Higgs boson, when coupled minimally to gravity, cannot provide a working model of inflation due to the large value of the coupling constant, $\lambda \simeq 0.1$, in the potential

$$V(\phi) = \frac{\lambda}{4}(\phi^2 - \sigma^2)^2, \quad (53)$$

where σ is the vacuum expectation value of the Higgs field (31). Indeed, $\lambda \simeq 0.1$ is many orders of magnitude larger than the CMB-constrained value $\lambda_c \simeq 1.43 \times 10^{-13}$ in the canonical framework (see Appendix A). Additionally, the potential (53) gives too small a value for the inflationary scalar spectral index n_s and too large a value for the tensor-to-scalar ratio r , to be in accord with observations.

However, the situation changes when one examines the potential (53) in the noncanonical framework. The expression for the inflationary scalar spectral index now becomes [14]

$$n_s = 1 - \left(\frac{\gamma + 4}{N_e \gamma + 2}\right), \quad (54)$$

where

$$\gamma \equiv \frac{2(3\alpha - 2)}{2\alpha - 1}. \quad (55)$$

Since γ increases from $\gamma = 2$ for $\alpha = 1$ to $\gamma = 3$ for $\alpha \gg 1$, the scalar spectral index *increases* from the canonical value $n_s = 0.951$ ($\alpha = 1, N_e = 60$) to $n_s = 0.962$ in noncanonical models (with $\alpha \gg 1$).

Similarly, one can show that the tensor-to-scalar ratio declines in noncanonical models. For the Higgs potential one gets [14]

$$r = \left(\frac{1}{\sqrt{2\alpha - 1}} \right) \left(\frac{32}{N_e \gamma + 2} \right), \quad (56)$$

which demonstrates that the value of r decreases with an increase in the noncanonical parameter α . Figure 17 shows n_S and r plotted as functions of α . One finds that $n_S \simeq 0.96$, $r < 0.1$ for $\alpha \geq 3$, which agrees well with CMB observations.

The relation between the value of the Higgs self-coupling $\lambda \simeq 0.1$ in the noncanonical framework and the corresponding canonical value λ_c is given by [14]

$$\lambda = 4 \left[\frac{32\lambda_c (N_e + 1)^3}{\sqrt{2\alpha - 1}} \left(\frac{\alpha}{4} \left(\frac{1 m_p^4}{6 M^4} \right)^{\alpha-1} \right)^{\frac{2}{3\alpha-2}} \left(\frac{1}{N_e \gamma + 2} \right)^{\frac{\gamma+4}{\gamma}} \right]^{\frac{3\alpha-2}{\alpha}}, \quad (57)$$

where consistency with CMB observations suggests $\lambda_c \sim 10^{-13}$.

Figure 18 describes the values of the noncanonical parameters α and M that yield $\lambda \simeq 0.1$ in Eq. (53)—the relation between M and α being provided by Eq. (57). In our subsequent analysis we choose $\alpha = 5$ for simplicity. This is shown by the black dot in Figs. 17(a) and 17(b). (The corresponding value of M is shown by the green dot in Fig. 18.)

As in the case of canonical scalar fields (20), one can rewrite the Friedman equation for noncanonical scalars (49) as follows:

$$R^2 = Y_{nc}^2 + X^2, \quad (58)$$

where

$$R = \sqrt{6} \frac{H}{m_p}, \quad X = \hat{\phi} \frac{\sqrt{2V(\phi)}}{m_p^2}, \quad (59)$$

$$Y_{nc} = \left[2(2\alpha - 1) \left(-\frac{F}{m_p^4} \right) \left(\frac{F}{M^4} \right)^{\alpha-1} \right]^{1/2}.$$

Therefore, by beginning at some initial value of R ($\equiv \sqrt{6}H/m_p$) one can set different initial conditions by varying X and Y_{nc} . Since X and Y_{nc} satisfy the constraint equation (58), they lie on the boundary of a circle.

We probe the robustness of this model to initial conditions by plotting its phase-space diagram (Y_{nc} vs X) and determining the region of initial conditions that give rise to adequate inflation ($N_e \geq 60$) for values of M and α that satisfy CMB constraints (shown by the green dot in Fig. 18). The phase-space diagram corresponding to an initial energy scale $H_i = 3 \times 10^{-3} m_p$ is shown in Fig. 19.

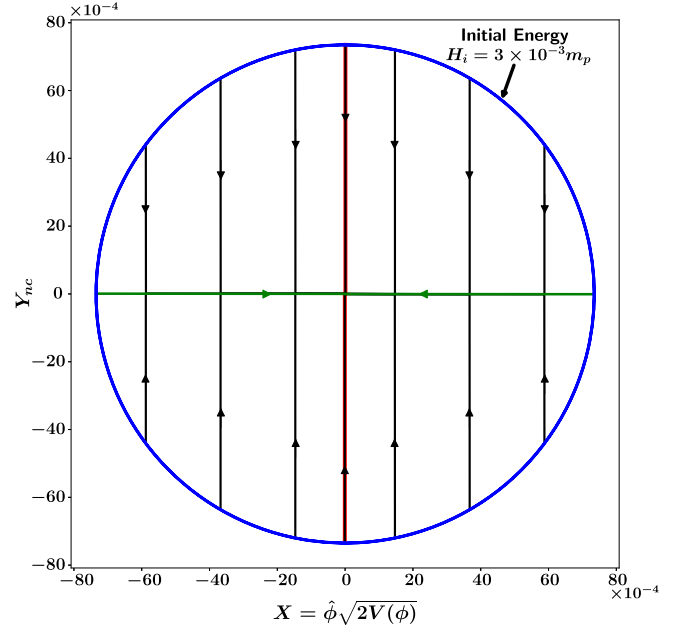


FIG. 19. This figure shows the phase-space of Higgs inflation in the noncanonical framework described by Eq. (53). Y_{nc} , given by Eq. (59), is plotted against X ($= \hat{\phi} \sqrt{2V(\phi)}$) for different initial conditions, all of which begin on the (blue) circle which represents the initial energy scale $H_i = 3 \times 10^{-3} m_p$. ($\hat{\phi} = \frac{\phi}{|\phi|}$ is the sign of field ϕ .) One finds that, beginning from the circle, different inflationary trajectories rapidly converge to one of the two inflationary separatrices (green horizontal lines) before proceeding towards the center, which corresponds to the minimum of the potential. The thin vertical central red band corresponds to the region in phase space that *does not* lead to adequate inflation. Note that this band is *very small*, which is indicative of the robustness of Higgs inflation in the noncanonical framework. The arc length of the red band, when divided by the circumference of the circle with radius $= \sqrt{6}H_i/m_p$, gives the fraction of initial conditions $\frac{2\Delta l_A}{l}$ that lead to inadequate inflation.

The fraction of initial conditions that give rise to inadequate inflation ($\frac{2\Delta l_A}{l}$) and partially adequate inflation ($\frac{2\Delta l_B}{l}$) are shown in Table V. (As earlier, a uniform distribution of X and Y_{nc} on the boundary of initial conditions has been assumed.) From this table one finds that the values of ϕ_A and ϕ_B associated with an initial energy scale H_i are much smaller than their counterparts for canonical inflation [see Figs. 20(a), 20(b), and 21]. This is a

TABLE V. Dependence of ϕ_A , ϕ_B , $\frac{\Delta l_A}{l}$, and $\frac{\Delta l_B}{l}$ on the initial energy scale H_i for noncanonical Higgs inflation. Here $l = 2\pi R \equiv 2\pi\sqrt{6}H_i/m_p$.

H_i (in m_p)	ϕ_A (in m_p)	ϕ_B (in m_p)	$2 \frac{\Delta l_A}{l}$	$2 \frac{\Delta l_B}{l}$
3×10^{-3}	8.74×10^{-3}	9.07×10^{-3}	1.48×10^{-3}	1.59×10^{-3}
3×10^{-2}	8.66×10^{-3}	8.99×10^{-3}	1.45×10^{-4}	1.57×10^{-4}
3×10^{-1}	8.58×10^{-3}	8.91×10^{-3}	1.43×10^{-5}	1.54×10^{-5}

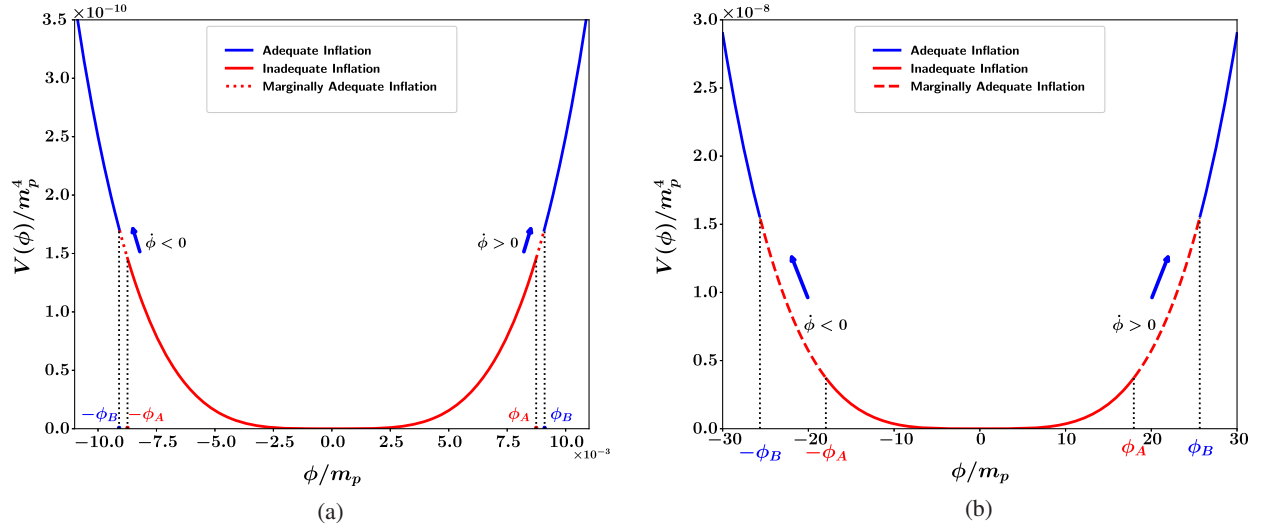


FIG. 20. Initial field values ϕ_i that lead to adequate inflation with $N_e \geq 60$ (blue), marginally adequate inflation (dashed red), and inadequate inflation (red) are schematically shown for the Higgs inflation with the quartic potential (53) (a) in the noncanonical framework and (b) in the canonical framework. The blue lines represent regions of adequate inflation. The red lines are either dashed or solid and correspond to the two possible initial directions of $\dot{\phi}_i$. The solid red line represents initial values of ϕ for which inflation is never adequate irrespective of the direction of $\dot{\phi}_i$. In the region shown by the dashed line one gets adequate inflation only when $\dot{\phi}_i$ points in the direction of increasing $V(\phi)$. We note that for the noncanonical case, the values of ϕ_A and ϕ_B are extremely small, as shown in Table V. (Only a small portion of the full potential is shown in this figure, which corresponds to the initial energy scale $H_i = 3 \times 10^{-3} m_p$.)

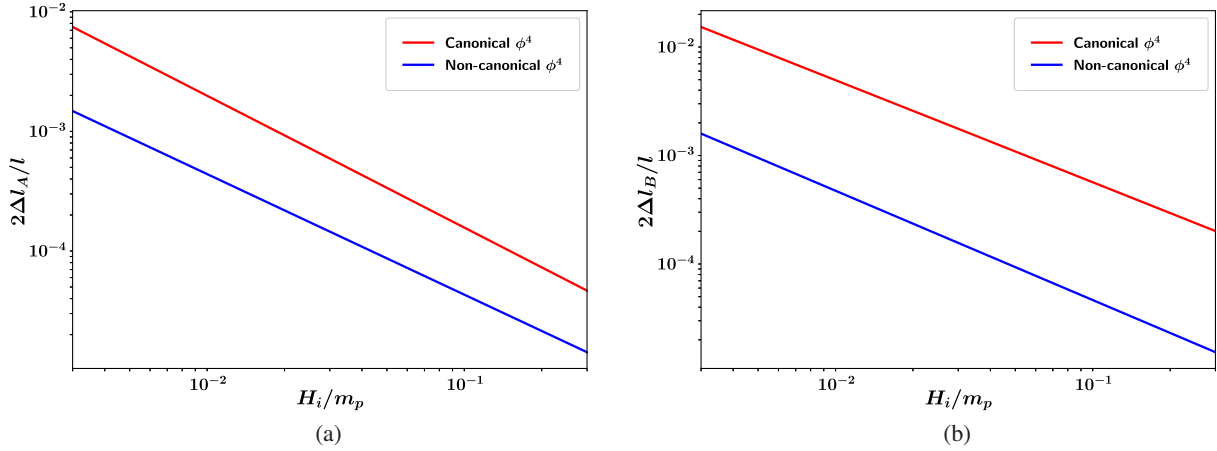


FIG. 21. This figure compares the values of (a) $\frac{\Delta_{l_A}}{l}$ and (b) $\frac{\Delta_{l_B}}{l}$ for canonical and noncanonical scalar fields with the potential $V(\phi) \propto \phi^4$. $\frac{\Delta_{l_A}}{l}$ and $\frac{\Delta_{l_B}}{l}$ are shown as functions of the initial energy scale of inflation H_i . The red and blue curves correspond to canonical and noncanonical quartic inflation, respectively. The smaller amplitude of the blue curve in both panels indicates that noncanonical inflation arises for a larger class of initial conditions than canonical inflation (red). The decrease in $\frac{\Delta_{l_A}}{l}$ and $\frac{\Delta_{l_B}}{l}$ with an increase in H_i is indicative of the fact that the set of initial conditions that give rise to adequate inflation (with $N_e \geq 60$) increases with the energy scale of inflation H_i .

consequence of the fact that for identical potentials, the slow-roll parameter in the noncanonical case is much smaller than its canonical counterpart ($\epsilon_{nc} \ll \epsilon_c$), which permits inflation to begin from *smaller values* of the inflaton field in the noncanonical case. We also find that the fraction of noninflationary initial conditions, $\frac{\Delta_{l_A}}{l}$, decreases with an increase of H_i , as expected.

In Fig. 21 we compare values of $\frac{\Delta_{l_A}}{l}$ and $\frac{\Delta_{l_B}}{l}$ for canonical inflation with $V_c(\phi) = \frac{\lambda_c}{4} \phi^4$ and noncanonical inflation¹¹ with $V(\phi) = \frac{\lambda}{4} \phi^4$, where λ and λ_c are related by Eq. (57).

¹¹Note that the Higgs potential in Eq. (53) can be rewritten as $V(\phi) \simeq \frac{\lambda}{4} \phi^4$, since $\sigma \ll m_p$.

We find that the values of $\frac{\Delta I_A}{I}$ and $\frac{\Delta I_B}{I}$ are significantly smaller for noncanonical inflation, which implies that inflation arises from a larger class of initial conditions in the noncanonical framework.

V. STAROBINSKY INFLATION

A. Action and potential in the Einstein frame

Starobinsky inflation [1] is based on the action

$$S = \int d^4x \sqrt{-g} \frac{m_p^2}{2} \left[R + \frac{1}{6m^2} R^2 \right], \quad (60)$$

where m is a mass parameter. The corresponding action in the Einstein frame is given by [39–41]

$$S_E = \int d^4x \sqrt{-g} \left[\frac{m_p^2}{2} \hat{R} - \frac{1}{2} \hat{g}^{\mu\nu} \partial_\mu \phi \partial_\nu \phi - V(\phi) \right], \quad (61)$$

where the inflaton potential is

$$V(\phi) = \frac{3}{4} m^2 m_p^2 \left(1 - e^{-\sqrt{\frac{2}{3}} \frac{\phi}{m_p}} \right)^2 \quad (62)$$

and $m = 1.13 \times 10^{-5} m_p$ is required from an analysis of scalar fluctuations [41] (see Appendix A). The potential (62) is shown in Fig. 22.

As shown in Fig. 22, the potential for Starobinsky inflation is asymmetric about the origin. One should

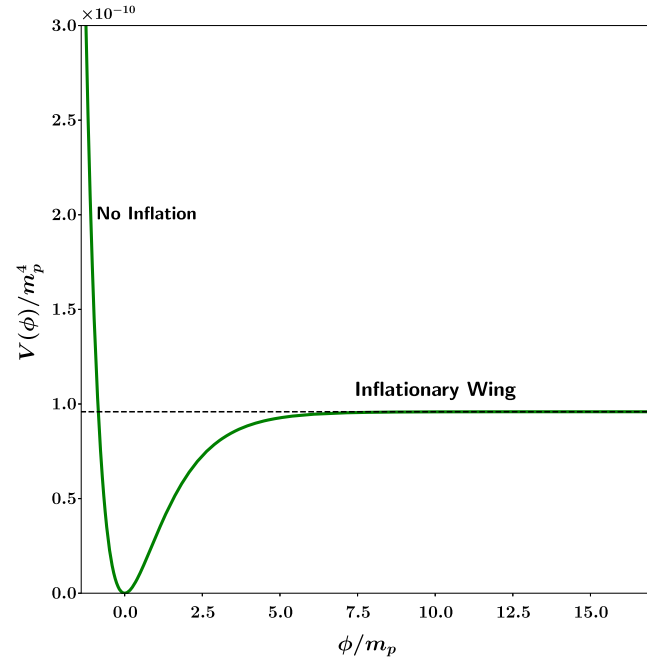


FIG. 22. The effective potential in Starobinsky inflation (62) is plotted in units of m_p^4 . The potential is asymmetric about the origin and has a steep left wing and plateau-like right wing. Inflation occurs along the flat plateau-like right wing, with the steep left wing being unable to sustain inflation.

note that the flat right wing of the potential has the same functional form as the Higgs inflation potential in the Einstein frame. However, the left wing of $V(\phi)$ is very steep. The slow-roll parameter for this potential is given by

$$\epsilon = \frac{4}{3} \left[\exp \left(\sqrt{\frac{2}{3}} \frac{\phi}{m_p} \right) - 1 \right]^{-2}.$$

Inflation occurs for $\epsilon \leq 1$, which corresponds to $\phi \geq 0.94 m_p$ and implies that no inflation can happen on the steep left wing of the potential (for which $\phi < 0$).

B. Generality of Starobinsky inflation

The distinctive properties of the Starobinsky potential discussed above result in an interesting phase space, which is shown in Figs. 24, 25, and 26 for an initial energy scale $H_i = 3 \times 10^{-3} m_p$. A deeper appreciation of this phase space is obtained by dividing the potential in Eq. (62) into four regions A, B, C, and D, as shown in Fig. 23. Note that adequate inflation is marked by blue arrows while

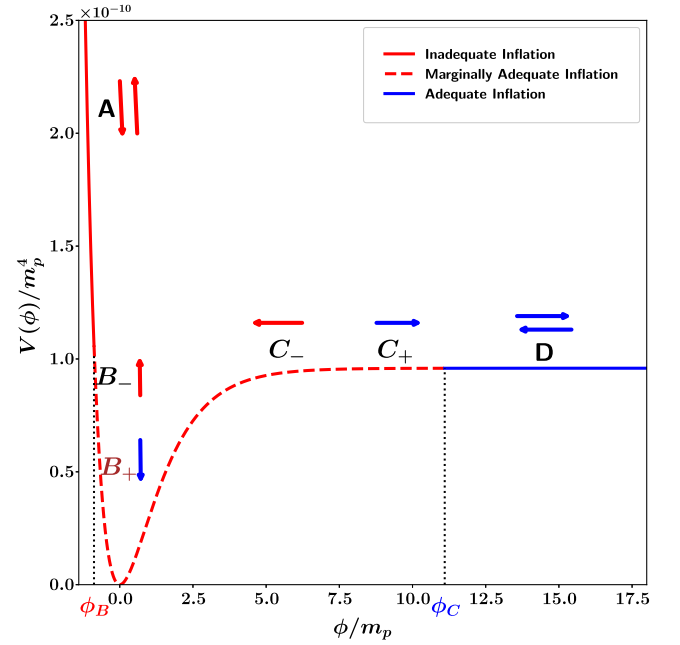


FIG. 23. This figure schematically shows initial field values that lead to adequate and inadequate Starobinsky inflation. The initial energy scale is $H_i = 3 \times 10^{-3} m_p$. The solid blue line represents the region of adequate inflation, while the solid red line displays the region of inadequate inflation. (Note that ϕ is unbounded on the right.) For initial field values lying in the interval $\phi_i \in [\phi_B, \phi_C]$ (red dashed line), one gets adequate inflation only if the initial velocity $\dot{\phi}_i$ is positive. This figure shows that it is easy for inflation to begin from the flat right wing of the potential. Note that only a small portion of the full potential is shown in this figure.

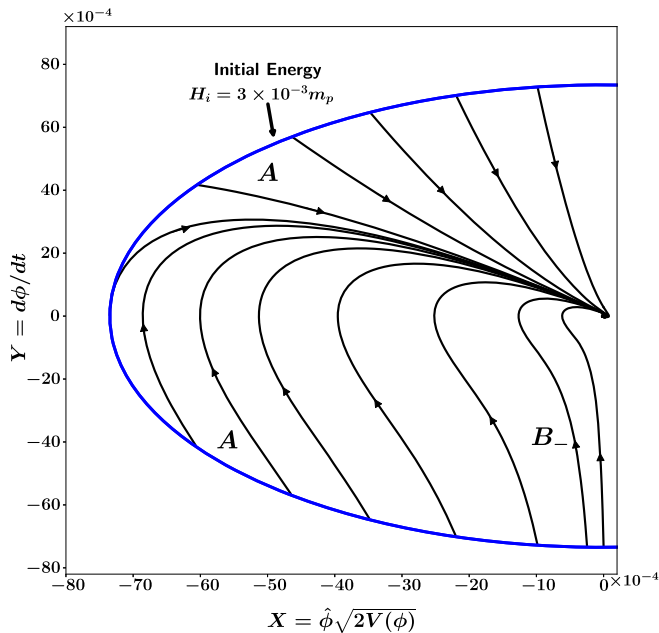


FIG. 24. This figure illustrates the phase space associated with the regions A and B_- on the steep left wing of the potential (62) illustrated in Fig. 23. As earlier, $Y = \dot{\phi}$ is plotted against $X = \hat{\phi} \sqrt{2V(\phi)}$ for the fixed initial energy scale $H_i = 3 \times 10^{-3} m_p$ (blue line). ($\hat{\phi} = \frac{\phi}{|\phi|}$ is the sign of field ϕ .) Note that the horizontal slow-roll inflationary separatrix is absent which reflects the fact that, by beginning from region A (and B_-) in Fig. 23, one cannot get adequate inflation from the steep left wing of the Starobinsky potential.

inadequate inflation is marked by red arrows (this notation has been consistently used throughout our paper). One gets adequate inflation in region D independently of the direction of $\dot{\phi}_i$ (illustrated by blue arrows in region D). Similarly, one gets inadequate inflation in region A independently of the direction of $\dot{\phi}_i$ (red arrows). However, one gets adequate inflation in region B (called B_+) and C (called C_+) provided $\dot{\phi}_i$ is positive (blue arrows), whereas negative $\dot{\phi}_i$ values in these regions (B_- and C_-) lead to inadequate inflation (red arrows). With this basic picture in mind, we now proceed to discuss the nature of the phase space in Figs. 24, 25, and 26.

The asymmetry of the potential (62) is reflected in the asymmetry of the phase space shown in Figs. 24, 25, and 26. The phase space associated with region A on the steep left wing of $V(\phi)$ does not exhibit slow-roll behavior and consequently does not possess an inflationary separatrix; see Fig. 24. The flat right wing of $V(\phi)$, on the other hand, has a slow-roll inflationary separatrix “ S ” (shown by the green line in Figs. 25 and 26), towards which most trajectories converge; see Figs. 25 and 26. Some of the lines beginning from the left wing with $\dot{\phi} > 0$ initially, represented by B_+ in Fig. 23 (the brown line in Fig. 26), are also able to meet the inflationary separatrix giving

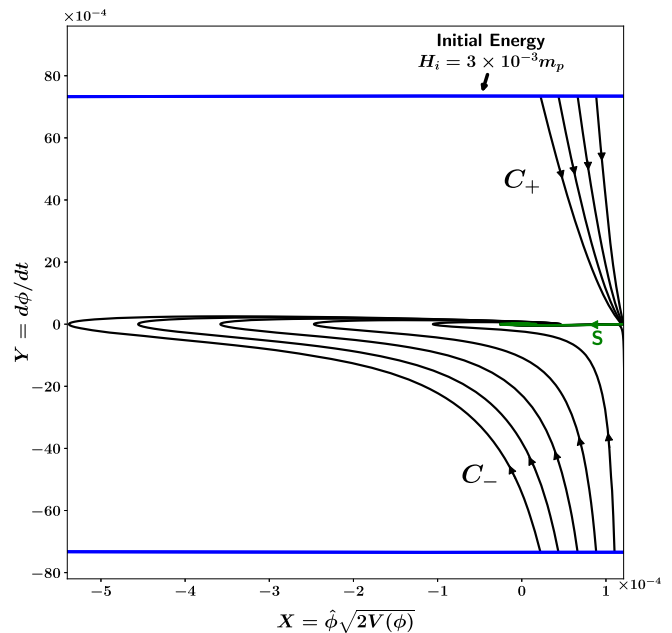


FIG. 25. This figure illustrates the phase space associated with the flat right wing of the potential (62). $Y = \dot{\phi}$ is plotted against $X = \hat{\phi} \sqrt{2V(\phi)}$ for the fixed initial energy scale $H_i = 3 \times 10^{-3} m_p$ (denoted by blue lines at the boundary). ($\hat{\phi} = \frac{\phi}{|\phi|}$ is the sign of field ϕ .) Note that trajectories beginning at the boundary with $\dot{\phi}_i > 0$ (region C_+ in Fig. 23) converge to the inflationary separatrix “ S ” before spiraling around the center (shown in detail in the next figure). By contrast, trajectories beginning on the right wing of $V(\phi)$ with $\dot{\phi}_i < 0$ in the region C_- in Fig. 23 do not lead to inflation.

rise to adequate inflation. These interesting features of Starobinsky inflation have been summarized in Fig. 23. In this figure, the solid blue line corresponding to $\phi_i \geq \phi_C$ shows trajectories that lead to adequate inflation *regardless of the initial direction of $\dot{\phi}_i$* . By contrast, the red region corresponding to $\phi_i \leq \phi_B$ reflects inadequate inflation. The intermediate region $\phi_i \in [\phi_B, \phi_C]$ leads to adequate inflation only when the initial velocity is positive, i.e., $\dot{\phi}_i > 0$ (dashed line). The dependence of ϕ_B and ϕ_C on the initial energy scale H_i is shown in Table VI.

From Table VI one observes that ϕ_B shifts to lower (more negative) values as the initial energy scale of inflation H_i is increased. This is indicative of the fact that inflation can begin even from the steep left wing of $V(\phi)$ provided the scalar field initially has a sufficiently large positive velocity, which would enable the inflaton to climb up the flat right wing and result in inflation.¹²

It may be noted that our results do not support some of the claims made in Ref. [12] that inflation in plateau-like

¹²Preinflationary initial conditions for Starobinsky inflation have also been studied in Ref. [42] in the context of loop quantum gravity.

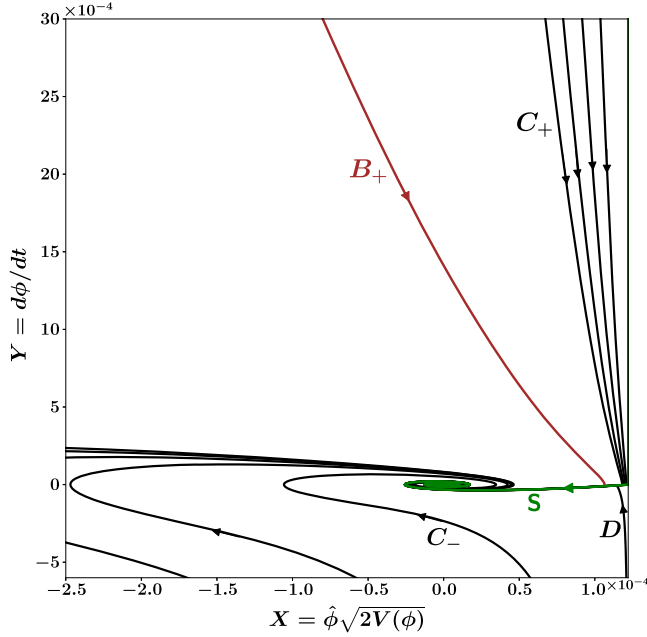


FIG. 26. A zoomed-in view of the phase space of Starobinsky inflation which highlights the existence of the slow-roll inflationary separatrix on the flat right wing (green line marked “S” in Fig. 23). Most trajectories beginning on the right wing (from regions C_+ and D) converge to “S” before spiraling in towards the minimum of $V(\phi)$. (The spirals correspond to post-inflationary oscillations.) Such an inflationary separatrix does not exist for the steep left wing of the potential. However, note the brown trajectory which is able to meet the inflationary separatrix on the right wing even though it begins from region B_+ of $V(\phi)$ (but with $\dot{\phi}_i > 0$), as shown in Fig. 23. The brown trajectory describes the motion of the field ϕ as it rolls up the potential.

potentials suffers from an *unlikelyness problem* since only a small range of initial field values lead to adequate inflation. The authors of Ref. [12] made this claim on the basis of a flat Mexican hat potential. Our analysis, based on more realistic models including Higgs inflation and Starobinsky inflation, has shown that, on the contrary, a fairly large range of initial field values (and initial energy scales) can give rise to adequate inflation, as illustrated in Figs. 16 and 23.

Finally, we would like to draw attention to the fact that the phase-space analysis performed here for Starobinsky inflation is likely to carry over to the E-model α -attractor potential [43], since the two potentials are qualitatively very similar.

TABLE VI. Dependence of ϕ_B and ϕ_C on the initial energy scale H_i for Starobinsky inflation.

H_i (in m_p)	ϕ_B (in m_p)	ϕ_C (in m_p)
3×10^{-3}	-0.28	11.11
3×10^{-2}	-2.16	12.99
3×10^{-1}	-4.04	14.87

VI. DISCUSSION

In this paper we have addressed the issue of the robustness of inflation to different choices of initial conditions. We considered a wide range of initial kinetic and potential terms $\frac{1}{2}\dot{\phi}_i^2$ and $V(\phi_i)$ for a given initial energy scale of inflation and determined the fraction of initial conditions that give rise to adequate inflation ($N_e \geq 60$). Our analysis has primarily focused on the following models: (i) chaotic inflation and its extensions such as monodromy inflation, (ii) Higgs inflation, and (iii) Starobinsky inflation. For class (i) we have shown that inflation becomes more robust for lower values of the exponent n in the inflaton potential $V \propto |\phi|^n$. This is illustrated in Fig. 11. Concerning class (ii), it is well known that Higgs inflation can arise from a nonminimal coupling of the Higgs field to the Ricci scalar. In this case the effective inflaton potential in the Einstein frame is asymptotically flat and has plateau-like features for large absolute values of the inflaton field. This is also true in the Einstein-frame representation of the Starobinsky potential, but in this case one of the wings of $V(\phi)$ is flat while the other is steep (and cannot sustain inflation). A remarkable feature shared by (nonminimally coupled) Higgs inflation and Starobinsky inflation is that one can get adequate inflation ($N_e \geq 60$) even if the inflaton begins to roll from the *minimum of the potential* ($\phi = 0$) and not from its periphery. This remarkable property is typical of asymptotically flat potentials and is not shared by the power-law potentials commonly associated with chaotic inflation. This new insight forms one of the central results of our paper.¹³

We also showed that inflation can be sourced by a Higgs-like field provided the Higgs has a noncanonical kinetic term. In this case noncanonical inflation is more robust, and arises for a larger class of initial conditions, than canonical inflation.

Using phase-space analysis, we have shown that the fraction of trajectories that inflate *increases* with an increase in the value of the energy scale at which inflation begins. This observation appears to be generic and applies to all of the models that have been studied in this paper.

One might note that our analysis in this paper assumed a specific measure on the space of initial conditions. Namely, we assumed that $X = \hat{\phi} \sqrt{2V(\phi)}$ ($\hat{\phi} = \frac{\phi}{|\phi|}$ is the sign of field ϕ) and $Y = \dot{\phi}$ are distributed uniformly at the boundary where initial conditions are set. Following this, we determined the degree of inflation. While this approach

¹³Our results for Higgs and Starobinsky inflation are likely to carry over to the (α -attractor-based) T-model [37] and E-model [43], respectively, due to the great similarity between the potentials of Higgs inflation and the T-model on the one hand, and Starobinsky inflation and the E-model on the other.

follows the seminal work of Ref. [10], it is also possible to construct alternative measures. For instance, one could assume instead that ϕ and $\dot{\phi}$ were distributed uniformly at the initial boundary. In this case the boundary will no longer be a circle, as it was for chaotic inflation in Fig. 1. Instead, its shape will crucially depend on the form of $V(\phi)$. However, we feel that as long as the initial phase-space distribution is not sharply peaked near specific values of ϕ_i and $\dot{\phi}_i$ the broad results of our analysis will remain in place. (In other words, we suspect that inflation is likely to remain generic for a large class of potentials, although we cannot prove this assertion.)

For the sake of simplicity, we have confined our analysis of inflationary initial conditions to a spatially flat FRW universe. The reader should note that by restricting ourselves to homogeneous and isotropic cosmologies we do not address the larger problem of inflation in an inhomogeneous and anisotropic setting. Indeed, the issue as to whether inflation can successfully arise in a universe that is either inhomogeneous or anisotropic (or both) is rather complex and has been discussed in several papers including the recent review [15]. In the case of a positive cosmological constant, it is well known that classical fluctuations in a FRW universe redshift and disappear and the space-time approaches de Sitter space asymptotically [44]. This result was extended to a “no-hair” theorem by a consideration of more general space-times including the spatially homogeneous but anisotropic Bianchi I–VIII family, which was shown to rapidly isotropize and (locally) approach de Sitter space in the future, provided all matter (with the exception of the cosmological constant) satisfies the strong energy condition [45]. The no-hair theorem was subsequently extended to inflationary cosmology in Ref. [46]. However, these studies primarily focused on anisotropic models and did not include the effects of inhomogeneity for which even a semianalytical treatment is difficult. A recent discussion of this issue within a numerical setting suggests that, for plateau-like potentials, inflationary expansion can arise even when the scale of inhomogeneity exceeds the Hubble length provided the mean spatial curvature is not positive [47] (also see Ref. [48]). The exception to this rule is associated with scalar field variations that exceed the inflationary plateau region and regions with large positive spatial curvature.¹⁴

¹⁴The latter can prove problematic for plateau-like potentials since, if the universe emerges from an initial Planck scale era with a large positive value of the curvature, then the latter would make the universe contract long before the energy density of the inflaton dropped to that of the inflationary plateau. A possible resolution of this problem is provided by potentials that, in addition to possessing a plateau-like region, also have monomial/exponential wings which allow inflation to begin from Planck-scale densities [49,50].

Overall it appears that the robustness of inflation (in relation to inhomogeneous initial data) is related to the fact that while strongly inhomogeneous overdense regions collapse to form black holes, underdense regions continue to expand, enabling inflation to eventually begin. It therefore appears that for inhomogeneous models the inflationary slow-roll regime is a local but not global attractor [15].

Finally, it is important to note that since the simplest models of inflation are not past-extendible [51], the origin of the inflationary scenario remains an important open question.

ACKNOWLEDGMENTS

A. V. T. is supported by RSF Grant No. 16-12-10401 and by the Russian Government Program of Competitive Growth of Kazan Federal University. A. V. T. is thankful to IUCAA, where this research work has been carried out, for the hospitality. S. S. M. thanks the Council of Scientific and Industrial Research (CSIR), India, for financial support as a senior research fellow. S. S. M. would also like to thank Surya Narayan Sahoo, Remya Nair, and Prasun Dutta for technical help in generating some of the figures. S. S. M. would like to thank Sanil Unnikrishnan for useful discussions and comments on the noncanonical Higgs inflation section.

APPENDIX A: THE VALUES OF n_s AND r FOR SEVERAL INFLATIONARY MODELS

For single-field slow-roll inflation, the amplitude of scalar fluctuations is given by [5]

$$\Delta_S^2 = \frac{1}{24\pi^2} \frac{V(\phi_*)}{m_p^4} \frac{1}{\epsilon(\phi_*)}, \quad (\text{A1})$$

where ϕ_* is the value of ϕ at N_e e -foldings before the end of inflation. CMB observations [16] imply $\Delta_S^2 = 2.2 \times 10^{-9}$ so that

$$\frac{1}{24\pi^2} \frac{V(\phi_*)}{m_p^4} \frac{1}{\epsilon(\phi_*)} = 2.2 \times 10^{-9}. \quad (\text{A2})$$

Similarly, for single-field slow-roll inflation, the scalar spectral index is given by [5]

$$n_s = 1 + 2\eta(\phi_*) - 6\epsilon(\phi_*), \quad (\text{A3})$$

and the tensor-to-scalar ratio is given by [5]

$$r = 16\epsilon(\phi_*). \quad (\text{A4})$$

TABLE VII. This table lists the CMB normalized value of the parameter, scalar spectral index n_S , and tensor-to-scalar ratio r for different single-field slow-roll inflationary models considered in this paper.

Model	$V(\phi)$	Parameter	n_S	r
Nonminimal Higgs	$V_0 \left(1 - e^{-\sqrt{\frac{2}{3}} \frac{ \phi }{m_p}}\right)^2$	$V_0 = 9.6 \times 10^{-11} m_p^4$	0.967	0.003
Starobinsky	$\frac{3}{4} m^2 m_p^2 \left(1 - e^{-\sqrt{\frac{2}{3}} \frac{\phi}{m_p}}\right)^2$	$m = 1.13 \times 10^{-5} m_p$	0.967	0.003
Fractional Monodromy	$V_0 \left \frac{\phi}{m_p}\right ^{2/3}$	$V_0 = 3.34 \times 10^{-10} m_p^4$	0.978	0.044
Linear Monodromy	$V_0 \left \frac{\phi}{m_p}\right $	$V_0 = 1.97 \times 10^{-10} m_p^4$	0.975	0.066
Quadratic Chaotic	$\frac{1}{2} m^2 \phi^2$	$m = 5.97 \times 10^{-6} m_p$	0.967	0.132
Quartic Chaotic	$\frac{\lambda_c}{4} \phi^4$	$\lambda_c = 1.43 \times 10^{-13}$	0.951	0.262

Values of the CMB normalized parameters n_S and r for some of the inflationary models discussed in this paper are listed in Table VII, assuming $N_e = 60$. The corresponding r vs n_S plot is shown in Fig. 27.

For Higgs inflation, substitution of the value $V_0 = 9.6 \times 10^{-11} m_p^4$ into Eq. (44) gives $\xi = 1.62 \times 10^4$ for the non-minimal coupling parameter, which is in agreement with Eq. (33).

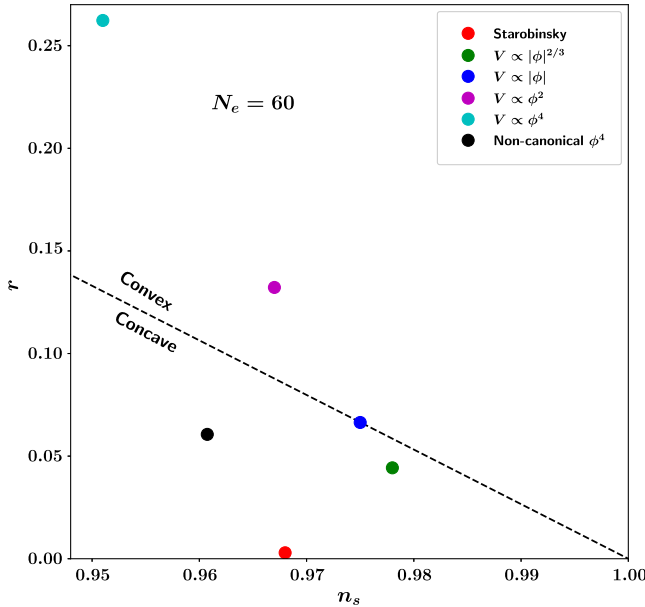


FIG. 27. The values of the tensor-to-scalar ratio r and the corresponding values of scalar spectral index n_S are plotted in this figure for different inflationary potentials considered in this paper corresponding to $N_e = 60$. Note that the values of r and n_S for Starobinsky inflation (62) and Higgs inflation in the nonminimal framework (43) are the same since both potentials have the same functional form as far as the flat inflationary wing is concerned. The value for the noncanonical $\lambda\phi^4$ potential has been determined assuming $\alpha = 5$ in Eq. (46).

APPENDIX B: JORDAN TO EINSTEIN FRAME TRANSFORMATION FOR HIGGS INFLATION

A derivation of Eqs. (38) and (39) is given below. Our derivation is similar to that given in Ref. [34]; however, we calculate the field transformation $\phi \rightarrow \chi$ explicitly. We begin with the Jordan frame action (29), namely,

$$S_J = \int d^4x \sqrt{-g} \left[f(\phi) R - \frac{1}{2} g^{\mu\nu} \partial_\mu \phi \partial_\nu \phi - U(\phi) \right], \quad (\text{B1})$$

which is described by the metric $g_{\mu\nu}$. The Einstein frame is described by $\hat{g}_{\mu\nu}$, where

$$\hat{g}_{\mu\nu} = \Omega^2 g_{\mu\nu}, \quad (\text{B2})$$

with the conformal factor being given by

$$\Omega^2 = \frac{2}{m_p^2} f(\phi) = 1 + \frac{\xi \phi^2}{m_p^2}. \quad (\text{B3})$$

Furthermore, $\sqrt{-g}$ transforms as

$$\sqrt{-g} \rightarrow \sqrt{-\hat{g}} = \Omega^4 \sqrt{-g} \quad (\text{B4})$$

and the Ricci scalar transforms as

$$R \rightarrow \hat{R} = \frac{1}{\Omega^2} \left[R - \frac{1}{\Omega} \square \Omega \right], \quad (\text{B5})$$

where

$$\square \Omega = \frac{1}{\sqrt{-g}} \partial_\mu (\sqrt{-g} g^{\mu\nu} \partial_\nu \Omega).$$

As a result, the action (B1) transforms to

$$S = \int d^4x \sqrt{-\hat{g}} \left[\frac{m_p^2}{2} \hat{R} - \frac{1}{2} \hat{g}^{\mu\nu} \left(\frac{1}{\Omega^2} \partial_\mu \phi \partial_\nu \phi + \frac{6m_p^2}{\Omega^2} \partial_\mu \Omega \partial_\nu \Omega \right) - \frac{U(\phi)}{\Omega^4} \right]. \quad (\text{B6})$$

Notice that the coupling of the scalar field to gravity has become minimal. However, the kinetic term is noncanonical. In order to change this to the canonical form one redefines the field $\phi \rightarrow \chi$ such that

$$\begin{aligned} & \frac{1}{2} \hat{g}^{\mu\nu} \left(\frac{1}{\Omega^2} \partial_\mu \phi \partial_\nu \phi + \frac{6m_p^2}{\Omega^2} \partial_\mu \Omega \partial_\nu \Omega \right) + \frac{U(\phi)}{\Omega^4} \\ &= \frac{1}{2} \hat{g}^{\mu\nu} \partial_\mu \chi \partial_\nu \chi + V(\chi), \end{aligned} \quad (\text{B7})$$

where

$$V(\chi) = \frac{U[\phi(\chi)]}{\Omega^4}. \quad (\text{B8})$$

Consequently, the action in the Einstein frame becomes

$$S_E = \int d^4x \sqrt{-\hat{g}} \left[\frac{m_p^2}{2} \hat{R} - \frac{1}{2} \hat{g}^{\mu\nu} \partial_\mu \chi \partial_\nu \chi - V(\chi) \right].$$

Note that by assuming a homogeneous and isotropic space-time one can drop the spatial derivative terms in Eq. (B7) to get

$$\begin{aligned} \frac{1}{\Omega^2} [\dot{\phi}^2 + 6m_p^2 \dot{\Omega}^2] = \dot{\chi}^2 &\Rightarrow \frac{1}{\Omega^2} \left[\dot{\phi}^2 + 6m_p^2 \left(\frac{\partial \Omega}{\partial \phi} \right)^2 \dot{\phi}^2 \right] \\ &= \left(\frac{\partial \chi}{\partial \phi} \right)^2 \dot{\phi}^2 \Rightarrow \left(\frac{\partial \chi}{\partial \phi} \right)^2 \\ &= \frac{1}{\Omega^4} \left[\Omega^2 + \frac{6\xi^2 \phi^2}{m_p^2} \right] \Rightarrow \frac{\partial \chi}{\partial \phi} \\ &= \pm \frac{1}{\Omega^2} \sqrt{\Omega^2 + \frac{6\xi^2 \phi^2}{m_p^2}}, \end{aligned}$$

which corresponds to Eq. (39). Note that the \pm sign here leads to the symmetric potential in Fig. 16.

APPENDIX C: DERIVATION OF ASYMPTOTIC FORMS OF THE HIGGS POTENTIAL IN THE EINSTEIN FRAME

Equations (39) and (B8) can be rewritten as

$$\frac{\partial \chi}{\partial \phi} = \pm \frac{\sqrt{1 + \frac{\xi \phi^2}{m_p^2} + \frac{6\xi^2 \phi^2}{m_p^2}}}{1 + \frac{\xi \phi^2}{m_p^2}}, \quad (\text{C1})$$

$$V(\phi) = \frac{U[\phi(\chi)]}{\Omega^4} \simeq \frac{\frac{\lambda}{4} \phi^4}{\left(1 + \frac{\xi \phi^2}{m_p^2}\right)^2}. \quad (\text{C2})$$

Using these two equations we proceed to derive the following useful asymptotic formulas:¹⁵

- (1) For $\phi \ll \sqrt{\frac{2}{3}} \frac{m_p}{\xi}$ one finds $\frac{\partial \chi}{\partial \phi} \simeq \pm 1$, and consequently Eq. (C2) simplifies to

$$V(\chi) \simeq \frac{\lambda}{4} \chi^4. \quad (\text{C3})$$

- (2) For $\phi \gg \sqrt{\frac{2}{3}} \frac{m_p}{\xi}$ one finds $\frac{\partial \chi}{\partial \phi} \simeq \pm \frac{\sqrt{6\xi\phi}}{\Omega^2}$, where $\Omega^2 = 1 + \frac{\xi \phi^2}{m_p^2}$. Hence, in this case

$$\chi \simeq \pm \sqrt{\frac{3}{2}} m_p \log \Omega^2(\phi). \quad (\text{C4})$$

For $\sqrt{\frac{2}{3\xi^2}} \ll \frac{\phi}{m_p} \ll \frac{1}{\sqrt{\xi}}$ Eq. (C4) reduces to

$$\chi \simeq \pm \sqrt{\frac{3}{2}} \frac{\xi \phi^2}{m_p}, \quad (\text{C5})$$

and consequently the potential in Eq. (C2) acquires the form

$$V(\chi) \simeq \left(\frac{\lambda m_p^2}{6\xi^2} \right) \chi^2. \quad (\text{C6})$$

Finally, for $\frac{\sqrt{\xi}\phi}{m_p} \gg 1$ one finds, from Eq. (C4),

$$\phi \simeq \frac{m_p}{\sqrt{\xi}} \exp\left(\frac{\pm \chi}{\sqrt{6}m_p}\right), \quad (\text{C7})$$

where the $+$ sign is taken for $\chi > 0$ and the $-$ sign is taken for $\chi < 0$, since the above solution is valid only in the limit when $|\frac{\sqrt{\xi}\phi}{m_p}| \gg 1$. Consequently, we can rewrite our solution as

$$\phi \simeq \frac{m_p}{\sqrt{\xi}} \exp\left(\frac{|\chi|}{\sqrt{6}m_p}\right), \quad (\text{C8})$$

and the potential in Eq. (C2) is given by

$$V(\chi) \simeq \frac{\lambda m_p^4}{4\xi^2} \left(1 + \exp\left[-\sqrt{\frac{2}{3}} \frac{|\chi|}{m_p}\right] \right)^{-2}. \quad (\text{C9})$$

To summarize, the relation between χ and ϕ in the three asymptotic regions is given by

$$\frac{\chi}{m_p} = \begin{cases} \pm \frac{\phi}{m_p}, & \frac{\phi}{m_p} \ll \sqrt{\frac{2}{3\xi^2}}, \\ \pm \sqrt{\frac{3}{2}} \frac{\xi(\phi)}{m_p}, & \sqrt{\frac{2}{3\xi^2}} \ll \frac{\phi}{m_p} \ll \frac{1}{\sqrt{\xi}}, \\ \pm \sqrt{6} \log\left(\frac{\sqrt{\xi}\phi}{m_p}\right), & \frac{\phi}{m_p} \gg \frac{1}{\sqrt{\xi}}. \end{cases}$$

¹⁵This analysis has been carried out assuming $\xi = 1.62 \times 10^4 \gg 1$.

- [1] A. A. Starobinsky, *Phys. Lett.* **91B**, 99 (1980).
- [2] A. H. Guth, *Phys. Rev. D* **23**, 347 (1981).
- [3] A. D. Linde, *Phys. Lett.* **108B**, 389 (1982).
- [4] A. Albrecht and P. J. Steinhardt, *Phys. Rev. Lett.* **48**, 1220 (1982).
- [5] A. D. Linde, *Contemp. Concepts Phys.* **5**, 1 (1990); A. R. Liddle and D. H. Lyth, *Cosmological Inflation and Large Scale Structure* (Cambridge University Press, Cambridge, England, 2000); D. Baumann, [arXiv:0907.5424](https://arxiv.org/abs/0907.5424).
- [6] V. F. Mukhanov and G. V. Chibisov, *JETP Lett.* **33**, 532 (1981).
- [7] S. W. Hawking, *Phys. Lett.* **115B**, 295 (1982).
- [8] A. A. Starobinsky, *Phys. Lett.* **117B**, 175 (1982).
- [9] A. H. Guth and S.-Y. Pi, *Phys. Rev. Lett.* **49**, 1110 (1982).
- [10] V. A. Belinsky, L. P. Grishchuk, I. M. Khalatnikov, and Y. B. Zeldovich, *Phys. Lett.* **155B**, 232 (1985).
- [11] V. A. Belinsky, H. Ishihara, I. M. Khalatnikov, and H. Sato, *Prog. Theor. Phys.* **79**, 676 (1988).
- [12] A. Ijjas, P. J. Steinhardt, and A. Loeb, *Phys. Lett. B* **723**, 261 (2013).
- [13] A. D. Linde, *Found. Phys.* **48**, 1246 (2018).
- [14] S. Unnikrishnan, V. Sahni, and A. Toporensky, *J. Cosmol. Astropart. Phys.* **08** (2012) 018.
- [15] R. Brandenberger, *Int. J. Mod. Phys. D* **26**, 1740002 (2017).
- [16] P. A. R. Ade *et al.* (Planck Collaboration), *Astron. Astrophys.* **594**, A20 (2016).
- [17] G. N. Felder, A. V. Frolov, L. Koffman, and A. D. Linde, *Phys. Rev. D* **66**, 023507 (2002).
- [18] A. D. Linde, *Phys. Lett.* **129B**, 177 (1983).
- [19] A. D. Linde, *Prog. Theor. Phys. Suppl.* **163**, 295 (2006).
- [20] E. Silverstein and A. Westphal, *Phys. Rev. D* **78**, 106003 (2008).
- [21] L. McAllister, E. Silverstein, and A. Westphal, *Phys. Rev. D* **82**, 046003 (2010).
- [22] K. Harigaya, M. Ibe, K. Schmitz, and T. T. Yanagida, *Phys. Lett. B* **720**, 125 (2013).
- [23] K. Harigaya, M. Ibe, K. Schmitz, and T. T. Yanagida, *Phys. Lett. B* **733**, 283 (2014).
- [24] K. Harigaya, M. Ibe, K. Schmitz, and T. T. Yanagida, *Phys. Rev. D* **90**, 123524 (2014).
- [25] R. Flauger, L. McAllister, E. Pajer, A. Westphal, and G. Xu, *J. Cosmol. Astropart. Phys.* **06** (2010) 009.
- [26] M. A. Amin, R. Easther, H. Finkel, R. Flauger, and M. P. Hertzberg, *Phys. Rev. Lett.* **108**, 241302 (2012).
- [27] C. Germani and A. Kehagias, *Phys. Rev. Lett.* **105**, 011302 (2010); *J. Cosmol. Astropart. Phys.* **05** (2010) 019; *Phys. Rev. Lett.* **106**, 161302 (2011); C. Germani and Y. Yatanabe, *J. Cosmol. Astropart. Phys.* **07** (2011) 031; S. Tsujikawa, *Phys. Rev. D* **85**, 083518 (2012).
- [28] F. L. Bezrukov and M. Shaposhnikov, *Phys. Lett. B* **659**, 703 (2008).
- [29] R. Fakir and W. G. Williams, *Phys. Rev. D* **41**, 1783 (1990).
- [30] F. L. Bezrukov, D. Gorbunov, and M. Shaposhnikov, *J. Cosmol. Astropart. Phys.* **06** (2009) 029.
- [31] J. Garca-Bellido, D. G. Figueroa, and J. Rubio, *Phys. Rev. D* **79**, 063531 (2009).
- [32] D. P. George, S. Mooij, and M. Postma, *J. Cosmol. Astropart. Phys.* **02** (2014) 024.
- [33] Y. Ema, R. Jinno, K. Mukaida, and K. Nakayama, *J. Cosmol. Astropart. Phys.* **02** (2017) 045.
- [34] D. I. Kaiser, *Phys. Rev. D* **81**, 084044 (2010).
- [35] A. Salvio and A. Mazumdar, *Phys. Lett. B* **750**, 194 (2015).
- [36] A. Salvio, *Phys. Lett. B* **780**, 111 (2018).
- [37] R. Kallosh and A. Linde, *J. Cosmol. Astropart. Phys.* **07** (2013) 002.
- [38] V. Mukhanov and A. Vikman, *J. Cosmol. Astropart. Phys.* **02** (2006) 004.
- [39] B. Whitt, *Phys. Lett.* **145B**, 176 (1984).
- [40] K. I. Maeda, *Phys. Rev. D* **37**, 858 (1988).
- [41] D. S. Gorbunov and A. G. Panin, *Phys. Lett. B* **743**, 79 (2015).
- [42] B. Bonga and B. Gupt, *Phys. Rev. D* **93**, 063513 (2016).
- [43] R. Kallosh, A. Linde, and D. Roest, *J. Cosmol. Astropart. Phys.* **11** (2013) 198.
- [44] G. W. Gibbons and S. W. Hawking, *Phys. Rev. D* **15**, 2738 (1977); S. W. Hawking and I. G. Moss, *Phys. Lett.* **110B**, 35 (1982); W. Boucher and G. W. Gibbons, in *The Very Early Universe*, edited by G. W. Gibbons, S. W. Hawking, and S. T. C. Siklos (Cambridge University Press, Cambridge, England, 1983).
- [45] R. M. Wald, *Phys. Rev. D* **28**, 2118 (1983); A. A. Starobinsky, *JETP Lett.* **37**, 66 (1983).
- [46] I. Moss and V. Sahni, *Phys. Lett. B* **178**, 159 (1986); V. Sahni and L. A. Kofman, *Phys. Lett. A* **117**, 275 (1986); **117**, 275 (1986); J. D. Barrow, *Phys. Lett. B* **180**, 335 (1986); **187**, 12 (1987); M. Mijic and J. A. Stein-Schabes, *Phys. Lett. B* **203**, 353 (1988); M. Mijic, M. S. Morris, and W.-M. Suen, *Phys. Rev. D* **39**, 1496 (1989); K. Olive, *Phys. Rep.* **190**, 307 (1990); J. H. Kung and R. H. Brandenberger, *Phys. Rev. D* **42**, 1008 (1990); D. S. Goldwirth, *Phys. Rev. D* **43**, 3204 (1991); D. S. Goldwirth and T. Piran, *Phys. Rep.* **214**, 223 (1992); Y. Kitada and Kei-ichi Maeda, *Phys. Rev. D* **45**, 1416 (1992); *Classical Quantum Gravity* **10**, 703 (1993); E. Calzetta and M. Sakellariadou, *Phys. Rev. D* **45**, 2802 (1992); R. Maartens, V. Sahni, and T. D. Saini, *Phys. Rev. D* **63**, 063509 (2001); C. Pitrou, T. S. Pereira, and J.-P. Uzan, *J. Cosmol. Astropart. Phys.* **04** (2008) 004; I. Y. Aref'eva, N. V. Bulatov, L. V. Joukovskaya, and S. Y. Vernov, *Phys. Rev. D* **80**, 083532 (2009); H.-C. Kim and M. Minamitsuji, *Phys. Rev. D* **81**, 083517 (2010); **82**, 109904(E) (2010); H.-C. Kim and M. Minamitsuji, *J. Cosmol. Astropart. Phys.* **03** (2011) 038; S. Hervik, D. F. Mota, and M. Thorsrud, *J. High Energy Phys.* **11** (2011) 146; A. Maleknejad, M. M. Sheikh-Jabbari, and J. Soda, *J. Cosmol. Astropart. Phys.* **01** (2012) 016; J. Soda, *J. Cosmol. Astropart. Phys.* **29** (2012) 083001; A. Maleknejad and M. M. Sheikh-Jabbari, *Phys. Rev. D* **85**, 123508 (2012); *Phys. Rep.* **528**, 161 (2013).
- [47] W. E. East, M. Kleban, A. Linde, and L. Senatore, *J. Cosmol. Astropart. Phys.* **09** (2016) 010.
- [48] A. H. Guth, D. I. Kaiser, and Y. Nomura, *Phys. Lett. B* **733**, 112 (2014).
- [49] K. Dimopoulos and M. Artymowski, *Astropart. Phys.* **94**, 11 (2017); M. Bastero-Gil, A. Berera, R. Brandenberger, I. G. Moss, R. O. Ramos, and J. G. Rosa, *J. Cosmol. Astropart. Phys.* **01** (2018) 002.
- [50] J. J. M. Carrasco, R. Kallosh, and A. Linde, *Phys. Rev. D* **92**, 063519 (2015); M. Artymowski, Z. Lalak, and M. Lewicki, *J. Cosmol. Astropart. Phys.* **01** (2017) 011.
- [51] A. Borde and A. Vilenkin, *Phys. Rev. Lett.* **72**, 3305 (1994).